7th IAA Planetary Defense Conference

26-30 April 2021, Online Event

Hosted by UNOOSA in collaboration with ESA

Session 6a: NEO Characterization

Chairs: Marina Brozovic | Stephen Lowry | Agata Rożek

Presenters: P. Pravec | J. de León | M. Fenucci | A. Sergeyev | M. Devogele

Photometric observations of the unrelaxed binary near-Earth asteroid (35107) 1991 VH in support of the NASA Janus space mission – Detection of a spin-orbit interaction

P. Pravec[a], P. Scheirich[a], D.J. Scheeres[b], J.W. McMahon [b], A.J. Meyer [b], P. Kušnirák[a], K. Hornoch[a], H. Kučáková[a], P. Fatka[a], R. McMillan[c], M. Brucker[c], J. Larsen[d], D. Fohring[e], R. Jedicke[e]

[a] Astronomical Institute AS CR, Ondřejov, Czech Republic
[b] University of Colorado, Boulder, CO, USA
[c] LPL, University of Arizona, Tucson, AZ, USA
[d] U.S. Naval Academy, Annapolis, MD, USA
[e] University of Hawaii, HI, USA

7th IAA Planetary Defense Conference
Vienna, Austria
2021 April 27

Discovery observations

Near-Earth asteroid 1991 VH – discovered by Rob McNaught from Siding Spring on November 9, 1991.

Binary nature of the asteroid – discovered by Pravec et al. (1998) from photometric observations taken with the 0.65-m telescope from Ondřejov during 1997 February 27 to April 4. They measured the basic parameters of the binary system (P_{prim}, P_{orb}, D_{sec}/D_{prim}, a) and estimated a non-zero eccentricity of the mutual orbit $e = 0.07 \pm 0.02$.

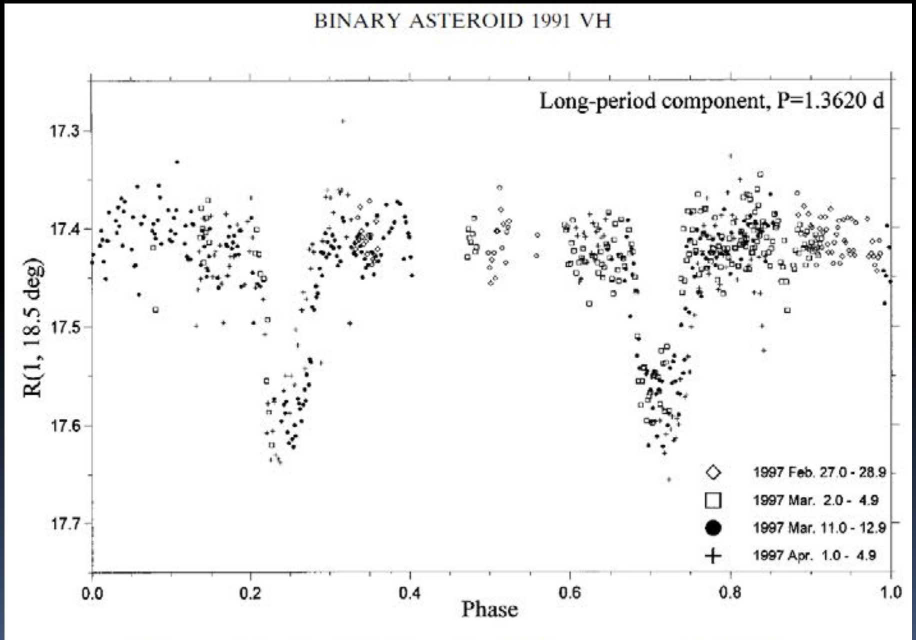

FIG. 5. Long-period lightcurve component. The epoch is JD 2450508.5.

Reference: Pravec et al., Icarus 133, 79-88 (1998)

Follow-up observations in 2003 and 2008

The asteroid had a favorable apparition in February 2003 → higher-quality follow-up observations taken with the Ondřejov 0.65-m.

Found a non-synchronous rotation of the secondary: P_{sec} = 12.836 ± 0.003 h (cf. P_{orb} = 32.67 h)

The secondary's equatorial elongation estimated a_s/b_s = 1.33 ± 0.10

Eccentricity refined to e = 0.05 ± 0.02 (3-σ error). Naidu et al. (2012) reported e = 0.05 from radar observations taken in 2008 as well, and they confirmed the non-synchronous secondary rotation.

Additional, shorter follow-up observations taken with the 0.65-m telescope in June/July 2008. The limited amount of data: a unique solution for P_{sec} not obtained, but the 2008 data didn't fit with the value 12.836 h observed in 2003 at all → Hint on that the secondary spin period is not constant.

(35107) 1991 VH is a unique unrelaxed asteroid binary system.

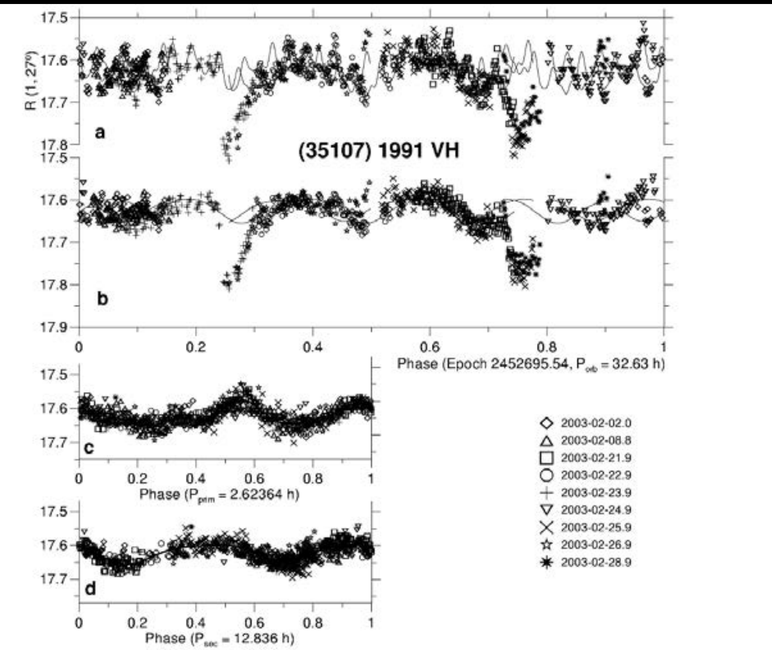

Fig. 12. Lightcurves of (35107) 1991 VH. (a) The original data showing the two rotational lightcurve components as well as the mutual events. The additive Fourier series with the periods of 2.6236 and 12.836 h was fitted to the rotation data. (b) The data showing the mutual events and the 12.836-h period variation after subtraction of the primary lightcurve component. (c) The primary lightcurve component. (d) The 12.836-h period lightcurve component (see text). $G = 0.26$.

References: Pravec et al., Icarus 181, 63–93 (2006). Pravec et al., Icarus 267, 267–295 (2016). Naidu et al., AAS/DDA Meeting 43, 7.07 (2012)

Target for the Janus mission

The unrelaxed binary asteroid (35107) 1991 VH has been selected as a target for the NASA Janus mission. (The other target for the mission is the ordinary, relaxed binary asteroid (175706) 1996 FG3.)

The Janus spacecraft will launch with the Psyche mission in 2022. Following a 4 year cruise (including one Earth gravity assist), the spacecraft will fly by the binaries before March 2026. During the flybys the spacecraft will image the target binary asteroids in the visible and IR, coming within 100 km of the asteroids.

The Janus mission will provide unique and unprecedented information on binary asteroids, allowing insight into their rubble pile properties, their formation and their evolution.

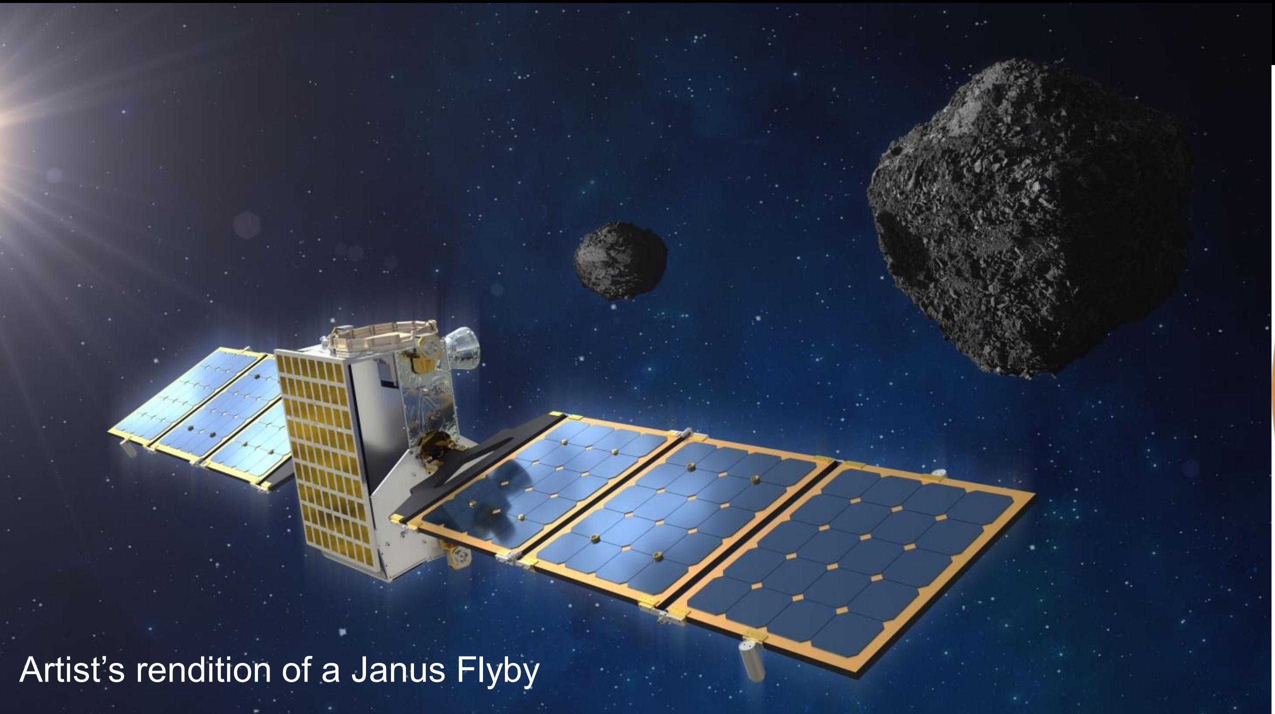

Artist's rendition of a Janus Flyby

Photometric campaign of 2020

The asteroid had another favorable apparition in January-March 2020.

We took extensive high-quality photometric observations with the 1.54-m telescope on La Silla (29 nights), the 0.9-m Spacewatch telescope (9 nights) and the 2.2-m telescope on Mauna Kea (3 nights) from 2020-01-19 to -03-16.

Found that both the secondary spin period P_{sec} and the orbit period P_{orb} changed again since the previous apparitions.

A small sample of the data:

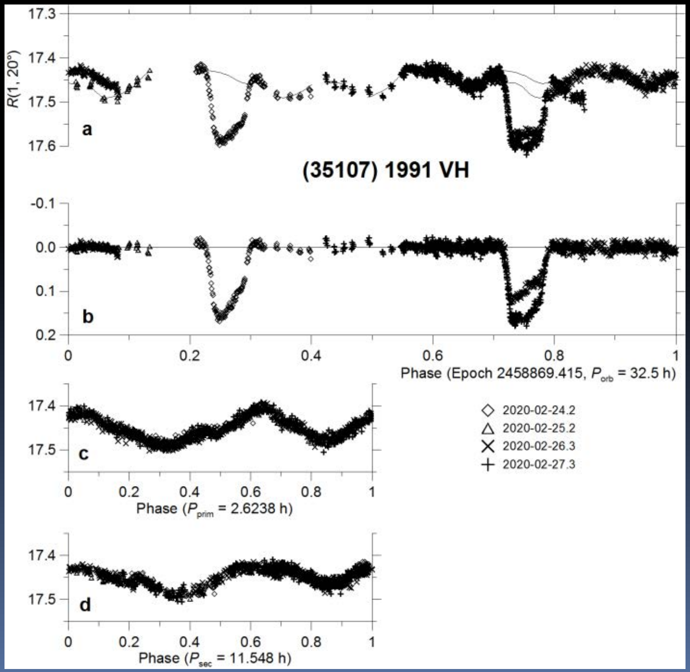

Mutual orbit precessing

Modeling of the mutual orbit in the 4 observed apparitions: A model with constant orbit pole cannot explain the observations → inclined and precessing orbit.

Instantaneous orbit pole constraints in the individual apparitions:

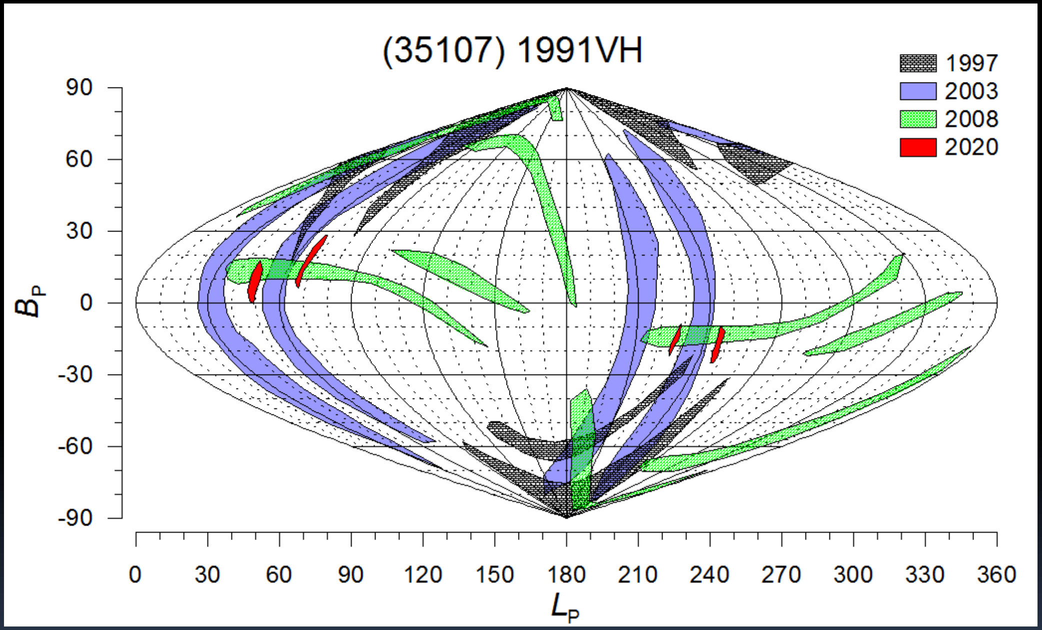

Plausible speculation: The inclination of the orbit wrt the primary's equator may be moderate only (several degrees up to a few ten degrees) – the orbit pole may precess not far from the instantaneous orbit pole constrained by the best 2020 data.

Secondary spin and orbit periods

Table 1: Secondary rotation and orbit periods of 1991 VH

Epoch UT	P_{sec} (h)	$P_{\mathrm{orb-syn}}$ (h)	$P_{\mathrm{orb-prograde}}$ (h)	$P_{\mathrm{orb-retrograde}}$ (h)
1997-03-17	n/a	32.69	32.68	32.72
2003-02-25	12.836	32.63	32.63	32.71
2008-07-01	(14.18)	32.80	32.84	32.76
2020-01-27	11.565	32.50	32.46	32.54
2020-02-18	11.777	dtto	dtto	dtto
2020-02-26	11.548	dtto	dtto	dtto
2020-03-02	11.612	dtto	dtto	dtto

3-σ uncertainties of P_{sec} are ≤ 0.02 h; the value in brackets is not unique.
3-σ uncertainties of the orbit periods are 0.01–0.07 h.
The orbit periods in 2020 were determined from all the data January-March.

Both the secondary rotation period P_{sec} and the orbit period P_{orb} show significant variations on an order of 1-2 h and 0.2 h, respectively, and they appear correlated.

Note: The observed (synodic) orbit periods $P_{\mathrm{orb\text{-}syn}}$ were affected by the synodic effect, its magnitude was between 0.00 and 0.08 h (median 0.04 h) for the individual epochs and orbit poles. We corrected the values assuming the orbit pole is either prograde or retrograde and it is close to *(L, B) ~ (57, +15)* or *(237, -15).*

Secondary spin and orbital energy

The apparent correlation between the secondary rotation period P_{sec} and the orbit period P_{orb} leads us to look into a balance between the secondary rotation energy and the orbit orbital energy.

Our hypothesis is that the sum of the secondary rotation and the orbital energy is constant:

$$E_{\rm sec} + E_{\rm orb} = \frac{1}{2} I_2 \omega_2^2 - G \frac{M_1 M_2}{2 a_{\rm orb}} = {\rm const.} \tag{1}$$

Using

$$I_2 = \frac{1}{5} M_2 (a_2^2 + b_2^2) \text{ and } n^2 a_{\rm orb}^3 = G(M_1 + M_2), \tag{2}$$

and approximating

$$M_1 \equiv V_1 \rho \doteq \frac{4}{3} \pi b_1^3 \rho, \tag{3}$$

we convert Eq. (1) to

$$\frac{1}{5} \left[\left(\frac{a_2}{b_2} \right)^2 + 1 \right] \omega_2^2 - \frac{\left(\frac{4}{3} \pi G \rho n \right)^{\frac{2}{3}}}{X^2 \sqrt[3]{1 + X^3}} = {\rm const.}, \tag{4}$$

where $X \equiv b_2/b_1$.

From Eq. (4), and as $n = 2\pi/P_{\rm orb}$ and $\omega_2 = 2\pi/P_{\rm sec}$, we can calculate a new $P_{\rm sec-fin}$ at a recent ('final') epoch with $P_{\rm orb-fin}$ from the original ('initial') values $P_{\rm sec-ini}$ and $P_{\rm orb-ini}$.

For 1991 VH, we have the secondary equatorial axis ratio $a_2/b_2 = 1.33$, the secondary-to-primary size ratio $X = 0.38$, and we assume $\rho = 2000\,{\rm kg/m^3}$. Then from the observed initial orbital and secondary spin periods
$P_{\rm orb-ini} = 32.67$ h and
$P_{\rm sec-ini} = 12.836$ h,
for the new observed orbital period
$P_{\rm orb-fin} = 32.50$ h
we get a new secondary spin period
$P_{\rm sec-fin} = 11.60$ h.

The predicted secondary period P_{sec} = 11.60 h for the 2020 epoch agrees with the observed values 11.548 to 11.777 h.

The observed changes of the secondary spin and orbit periods from 2003 to 2020 are consistent with an exchange of energy between the secondary rotation and orbital motion → spin-orbit interaction

Full Two Body Problem

Arbitrary masses in close proximity see significant spin-orbit coupling: Position and orientation of both asteroids are important.

The mutual orbit does not follow Keplerian dynamics. The semimajor axis and eccentricity are found using the observed positions instead of Kepler's laws.

Numeric simulations are done using the General Use Binary Asteroid Simulator[1]

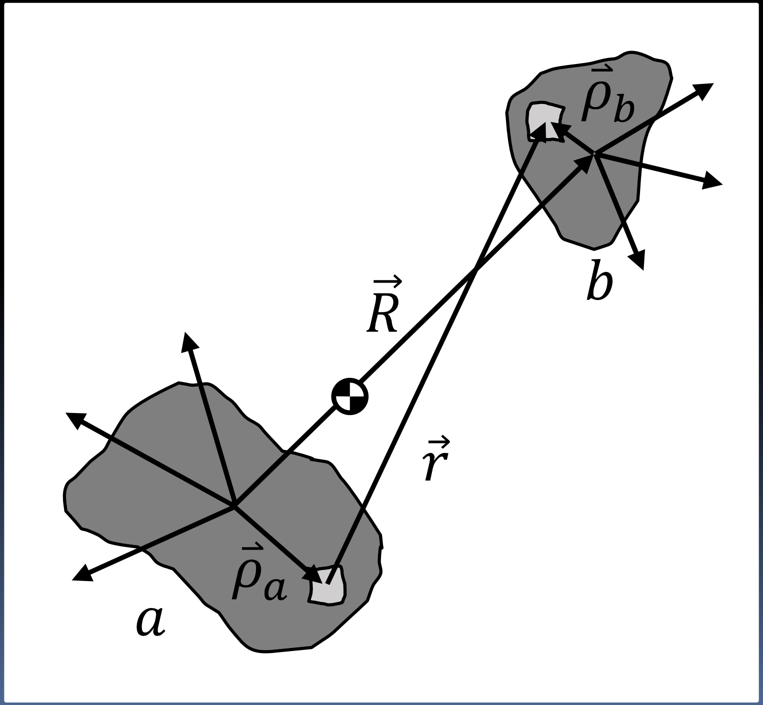

[1] https://github.com/alex-b-davis/gubas

1991 VH Numeric Simulations

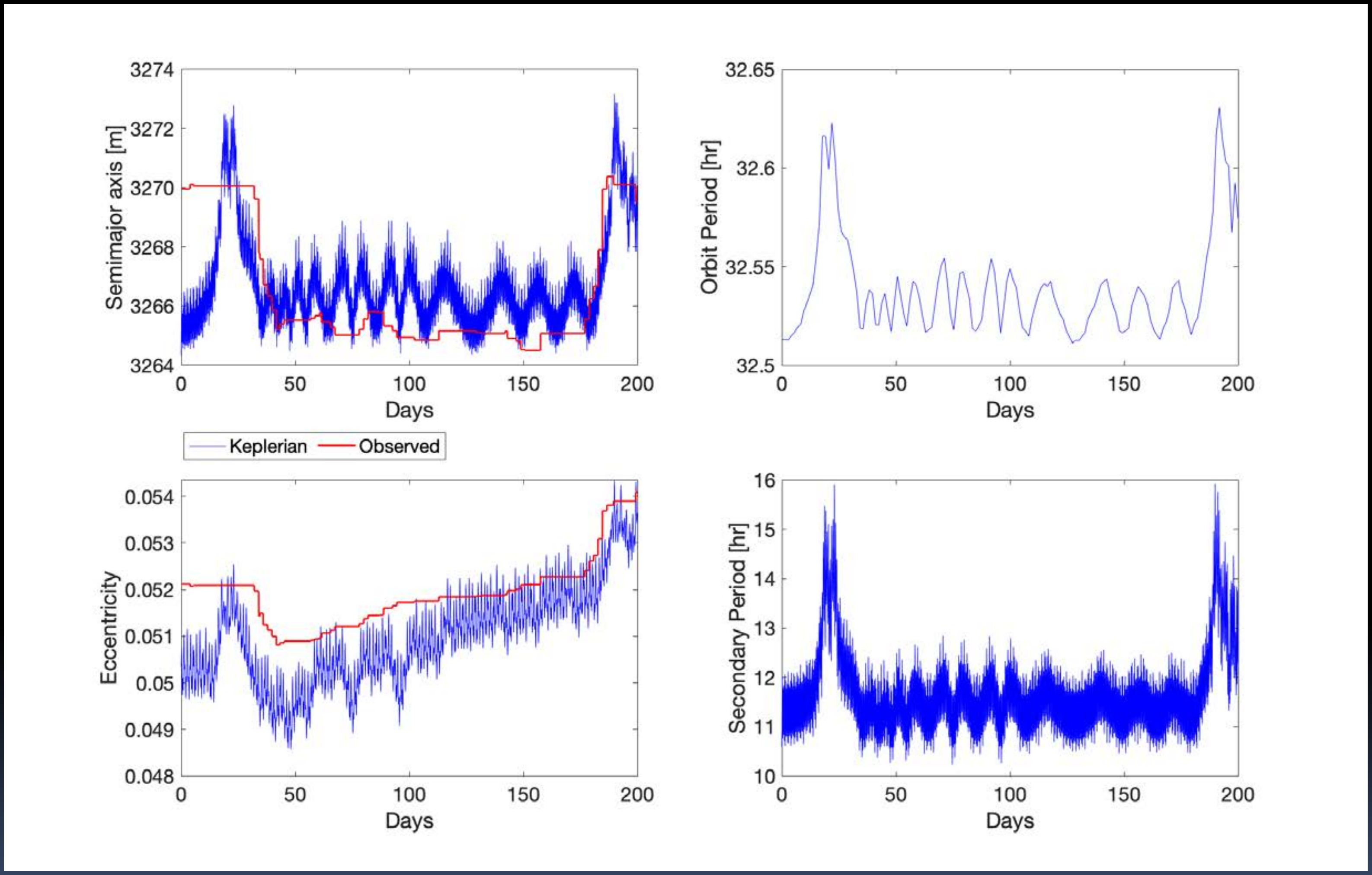

The jumps in orbit period and secondary spin period are correlated with the secondary tumbling in its orbit. The observed elements are calculated using a 3-day window of the separation.

Conclusions

The binary near-Earth asteroid (35107) 1991 VH is in an unrelaxed state with inclined (precessing) and eccentric orbit and non-synchronous secondary (satellite) rotation.

The secondary spin period and the orbital period appear correlated. The observed changes of the periods from 2003 to 2020 suggest a spin-orbit interaction.

More thorough simulations of the full two body problem needed to get a better understanding of the unrelaxed binary system.

7th IAA Planetary Defense Conference

26-30 April 2021, Online Event

Hosted by UNOOSA in collaboration with ESA

Characterization of NEAs in the frame of NHATS program using the 10.4m Gran Telescopio Canarias

Julia de León[1,2], Javier Licandro[1,2], Marcel Popescu[3], David Morate[1,2], Hissa Medeiros[1,2], Paul Abell[4], and Fabricio Pérez Toledo[5]

(1) Instituto de Astrofísica de Canarias, Tenerife (Spain)
(2) Departamento de Astrofísica, Universidad de La Laguna, Tenerife (Spain)
(3) Astronomical Institute of the Romanian Academy, Bucharest (Romania)
(4) NASA Johnson Space Center, Houston (USA)
(5) GRANTECAN, La Palma (Spain)

NASA Near-Earth Object Human Space Flight Accessible Targets Study: NHATS

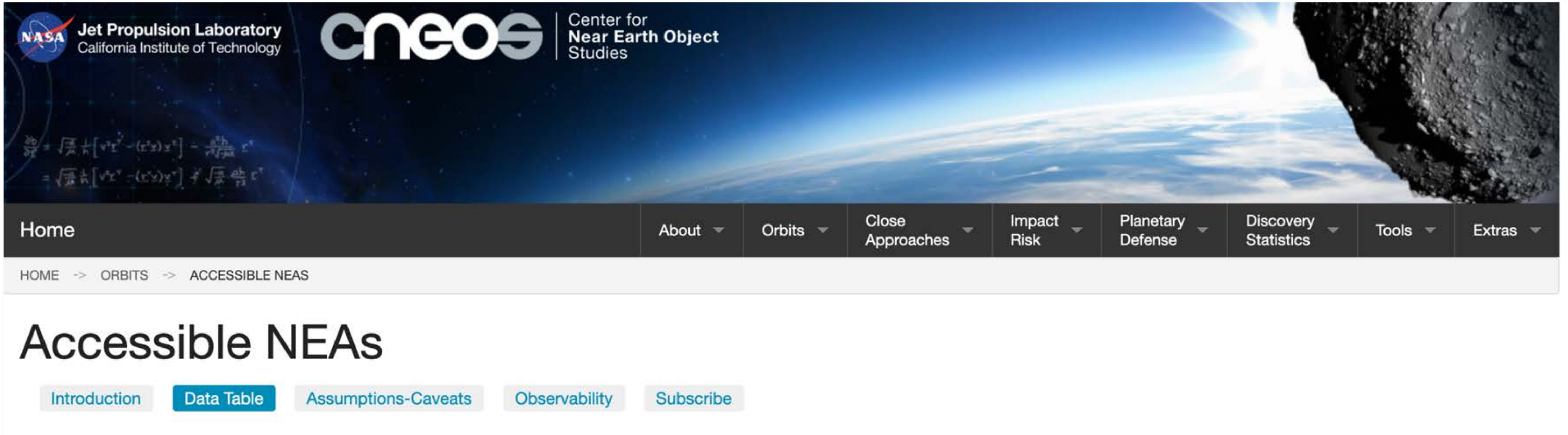

- NHATS began in September 2010 **<u>to identify any known NEOs that might be accessible by future human space flight missions</u>**.
- High-priority targets are identified and alerts are sent out to the observing community requesting observations.
- Best observed during discovery apparition --> need from fast response (in particular for small NEAs)
- Large aperture telescopes are best suited

Observing with the 10.4m Gran Telescopio Canarias (GTC)

Canary Islands (Spain)

The 10.4m Gran Telescopio Canarias (GTC) is located at the El Roque de Los Muchachos Observatory (La Palma), managed by the Instituto de Astrofísica de Canarias (IAC).

We started this observational program in 2014 for 3 semesters. It was resumed in 2019 and is currently on-going.

OSIRIS camera-spectrograph | 2 CCD detectors 2K x 4K | FOV 7.4’ x 7.4’ | Long-slit | R300 grism | $\delta\lambda$ ~ 0.001 µm | 0.48 – 0.92 µm

Observing with the 10.4m Gran Telescopio Canarias (GTC)

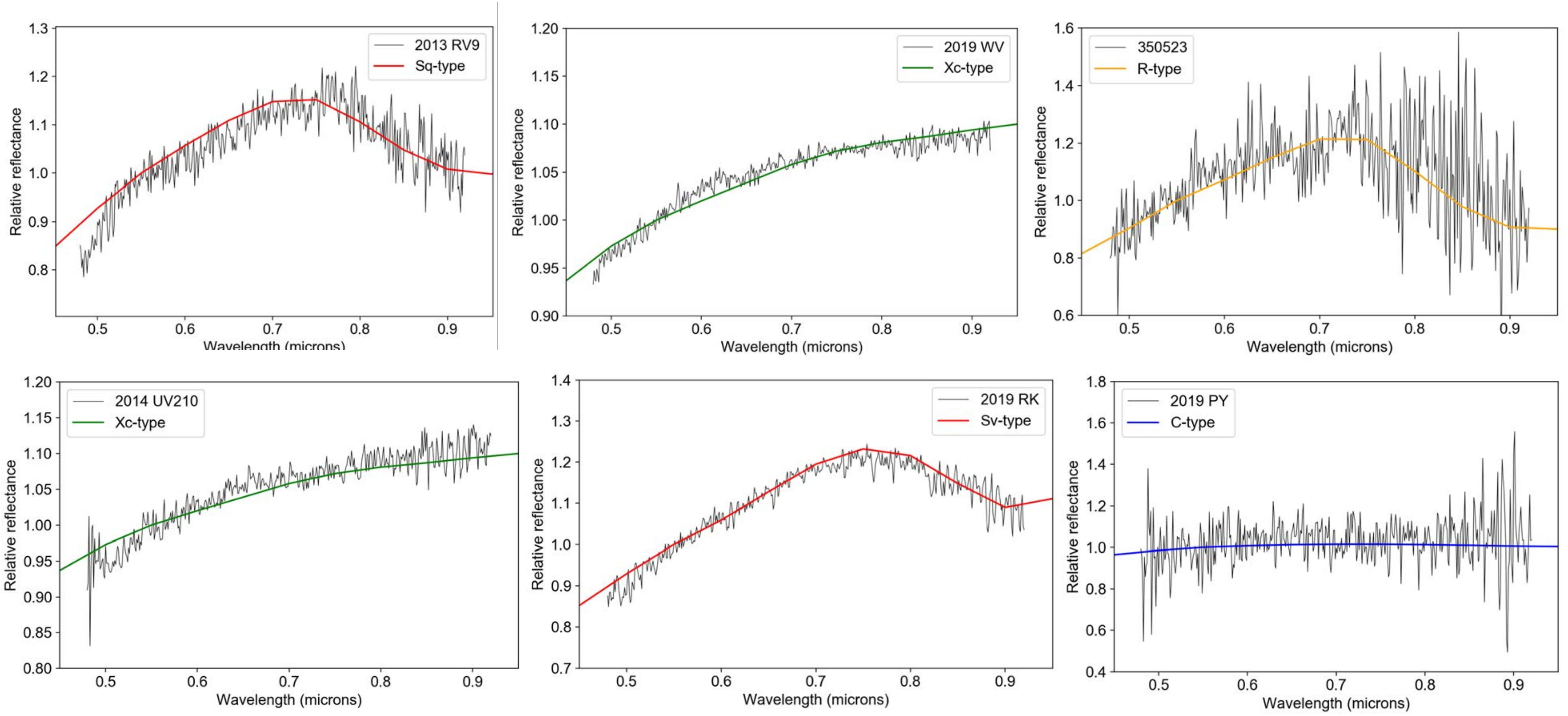

Observing with the 10.4m Gran Telescopio Canarias (GTC)

Asteroid	Discovery date[1]	Observation date	m_V	α (°)	H[1]	p_V[2]	Tax[3]	*D* (km)	Notes
350523	Mar 3, 2000	Jun 1, 2019	20.5	23.1	21.0	0.148	R	0.218	
2013 RV9	Sep 3, 2013	Mar 9, 2019	20.7	33.6	23.6	0.211	S	0.055	
2014 UV210	Oct 25, 2014	Dec 16, 2014	18.7	5.8	26.9	0.047	X	0.025	Fast rotator (< 1 h)
2015 BG92	Jan 19, 2015	Jan 26, 2015	18.6	25.6	25.1	0.048	D	0.058	Fast rotaror (< 0.2 h)
2015 DU	Feb 17, 2015	Feb 28, 2015	19.1	19.5	26.6	0.211	S	0.014	Fast rotator (< 0.1 h)
2017 PV25	Jul 24, 2017	Mar 10, 2019	20.7	18.0	24.7	0.129	Xc	0.042	
2019 JU5	May 4, 2019	Jun 2, 2019	20.7	31.5	24.0	0.211	S	0.045	
2019 UO1	Oct 19, 2019	Oct 28, 2019	21.0	15.5	25.0	0.050	C	0.059	
2019 WV	Nov 21, 2019	Nov 25, 2019	19.2	27.8	24.9	0.129	Xc	0.038	P_{rot} = 1.25 h
2019 YV	Dec 19, 2019	Dec 27, 2019	18.9	39.7	23.6	0.042	T	0.123	
…	…	…	…	…	…	…	…	…	

[1] *JPL Small-Body Database Browser (https://ssd.jpl.nasa.gov/sbdb.cgi#top) and IAU Minor Planet Center*

[2] *When no albedo information is available, we use the average albedo for the taxonomical class from Mainzer et al. (2011)*

[3] *Taxonomical classification is done using the M4AST on-line tool (http://spectre.imcce.fr/m4ast/index.php/index/home, Popescu et al. 2012)*

Some preliminary results

A total of 24 NEAs have been observed so far

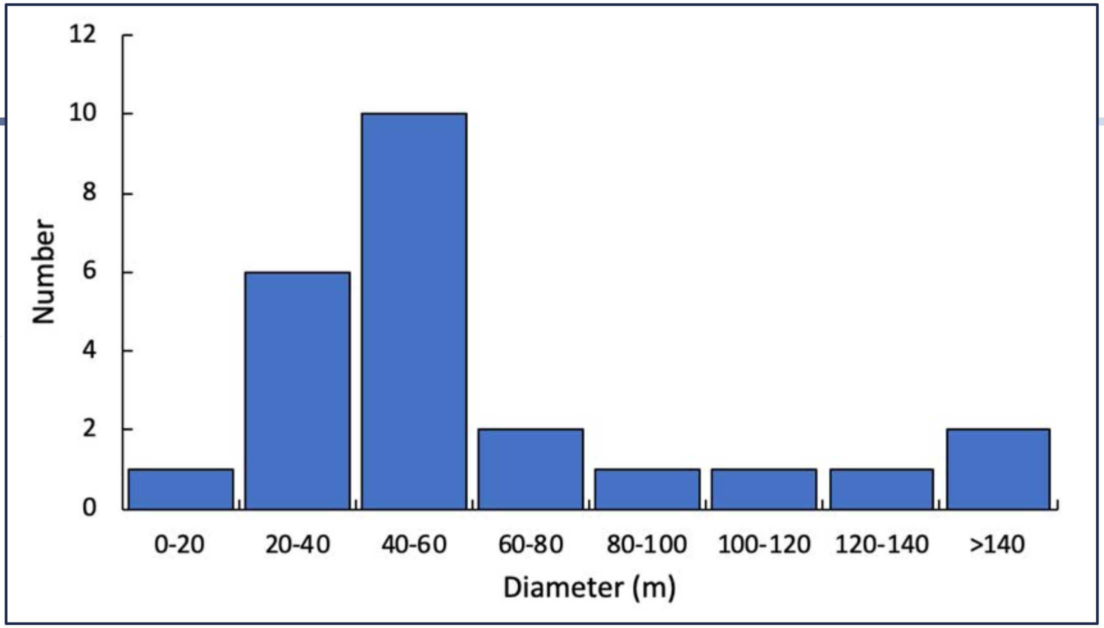

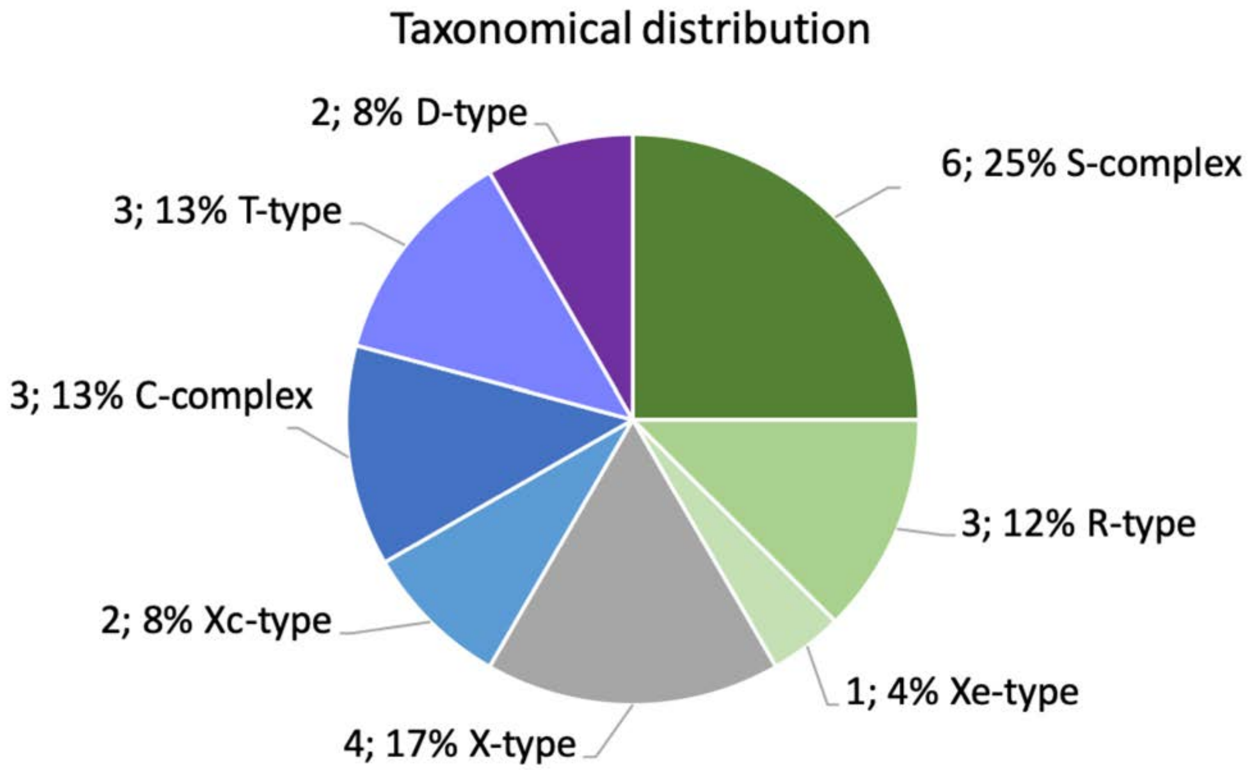

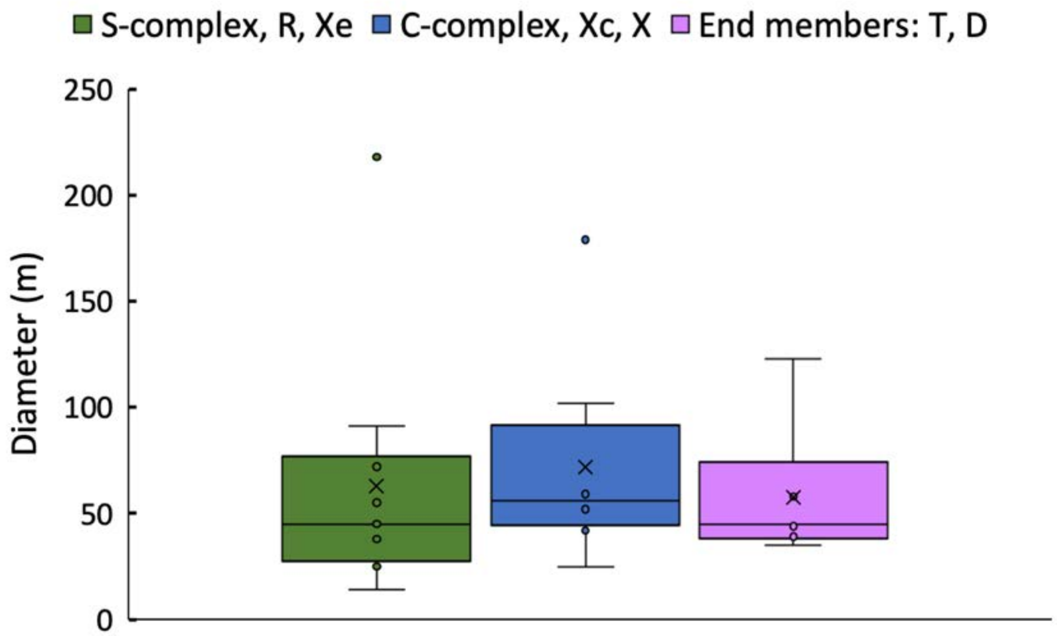

Conclusions

- We have an on-going observational program to obtain visible spectra of NEAs using the 10.4m Gran Telescopio Canarias (GTC), in the frame of the NHATS program.
- So far, we have observed 24 NEAs.
- We find a bit more primitive (59%) than rocky (41%) NEAs, and a total of 2 D-types and 3 T-types.
- The majority of the targets (83%) have diameters < 100m. Some of them are fast rotators (P_{rot} < 1h). We do not see any tendency between taxonomical classes and diameters.

The low thermal conductivity of the super-fast rotator (499998) 2011 PT

M. Fenucci[1], B. Novaković[1], D. Vokrouhlický[2], R. J. Weryk[3]

[1]University of Belgrade, [2]Charles University, [3]University of Hawaii

7$^{\text{th}}$ Planetary Defense Conference

26 - 30 April 2021

Motivation

It is supposed that:

- Small and fast rotators are **monolithic objects**
- Rocky monoliths have **high thermal inertia**
- High thermal inertia makes the Yarkovsky effect **less** effective

However:

- **Del Vigna et al. 2018** and **Greenberg et al. 2020** found small objects with fast Yarkovsky drift

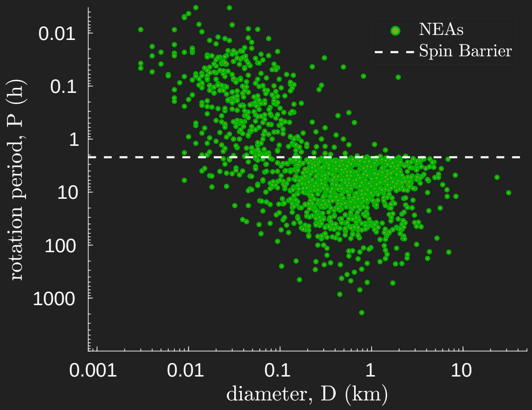

Case study: (499998) 2011 PT

Characteristics:

- $H \sim 24$ mag $\Rightarrow$ **D $\sim$ 35 m**
- $P \sim 11$ min
- **Yarkovsky effect** detected by
  - Del Vigna et al. 2018
  - Greenberg et al. 2020
  - JPL SBDB

Goal:

- Constrain the **thermal conductivity** (**thermal inertia**)

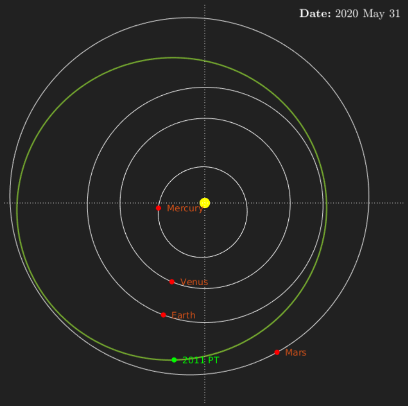

Methods: model vs. observed Yarkovsky drift

$$\left(\frac{\mathrm{da}}{\mathrm{dt}}\right)(\mathbf{a}, \mathbf{D}, \rho, \mathbf{K}, \mathbf{C}, \gamma, \mathbf{P}, \alpha, \varepsilon) = \left(\frac{\mathrm{da}}{\mathrm{dt}}\right)_{\mathsf{m}}$$

Parameters:

- **a** semimajor axis
- **D** diameter
- ρ density
- **K** thermal conductivity
- **C** heat capacity
- γ obliquity
- **P** rotation period

Method:

- Assume distributions for all the parameters but K
- Solve for K the model vs. observed equation
- Use a Monte Carlo method for statistical analysis

Results of the Monte Carlo simulations

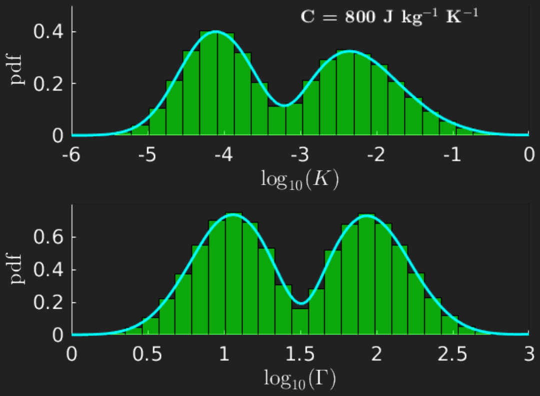

- The distributions are always **bimodal**
- **First peak** in K at around

$$\sim \mathbf{7 \cdot 10^{-5}} \text{ W m}^{-1} \text{ K}^{-1}$$

- **Second peak** in K at around

$$\sim \mathbf{5 \cdot 10^{-3}} \text{ W m}^{-1} \text{ K}^{-1}$$

- $P(K < 0.1 \text{ W m}^{-1} \text{ K}^{-1}) > 0.95$

Comparison with other asteroids

The estimated thermal inertia for 2011 PT is

$$11^{+7}_{-5} \text{ and } 88^{+90}_{-45}$$

Low thermal inertia is usually associated to **regolith**

Asteroid	D (km)	Γ (J m^{-2} K^{-1} s$^{-1/2}$)
Ceres	923	10 ± 10
Pallas	544	10 ± 10
Vesta	525	20 ± 15
Eros	17	150 ± 50
1950 DA	1.3	24 ± 20
Ryugu	0.87	225 ± 45
Bennu	0.49	310 ± 70
Itokawa	0.32	700 ± 200

Conclusions

- First evidence supporting the hypothesis that regolith can be retained on small and super-fast rotators (**Sanchez & Scheeres 2019**, *Icarus*)
- Large rocky boulders with low thermal inertia were found on **Bennu** and **Ryugu**. However, 2011 PT is an **E-type** asteroid.
- 2011 PT might be a rubble-pile, but it is highly unexpected

Future works and opened questions

- More studies and characterization of asteroids with $D < 100$ m are needed for the planning of *deflection* or *Asteroid Redirect* missions
- What are the processes and timescales of regolith formation on fast rotators?
- Is 2011 PT a good representative of the population of asteroids with $D < 100$ m?

7th IAA Planetry Defence Conference

Photometry of Near-Earth asteroids in the Sloan Digital Sky Survey

Alexey Sergeyev and Benoit Carry

Observatory de Cote d'Asur

April 17, 2021

Motivation

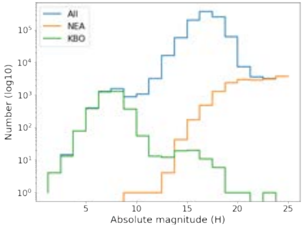

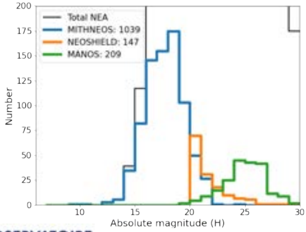

Asteroids distribution by size:

Dynamical class	Number*
Near-Earth	23,424
Mars-Crosser	19,339
Main Belt	919,004
Kuiper Belt	3,536
Total	995,628

*The Asteroid Orbital Elements Database

Known NEOs Taxonomy:

Campaign	Number
MANOS[1]	210
NEOSHIELD2[2]	147
MITHNEOS[3]	1,039
Total	1,380

[1] Devogèle et al.(2019)
[2] Perna et al.(2018)
[3] Binzel et al.(2019)

Why the SDSS?

- 14,555 deg^2 coverage area (1998-2008).
- 95% completeness sources in u,g,r,i,z filters up to 22.2 mag.
- Archive of the sources catalog and fits frames.
- Quasi-synchronous multi-band observations.

Sky coverage of the SDSS

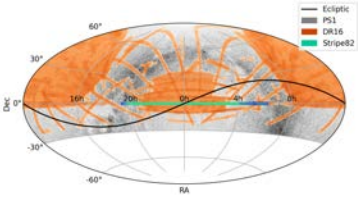

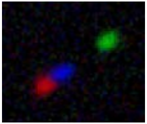

Figure: g(green), r(red), i(blue) image of the asteroid 1990 SP

A new SDSS catalog of Solar System Objects

- The **previous** Moving Object Catalog MOC4 (Ivezic+2002)
  - 471,569 moving objects
  - 220,101 linked with asteroids
  - 104,449 unique asteroids
  - $<$ 300 Near Earth asteroids

  Contains only **HALF** of available SDSS RUNs!

- The **new** SSOs SDSS catalog (Sergeyev and Carry 2021 submitted)
  - Repeated Ivezic query on all RUNs without fast moving rate limit
  - Query SkyBoT for known SSOs.
  - Extensive cross-match with PanSTARRS & Gaia

- The **new** Moving Object Catalog
  - 1,533,759 real moving objects!
  - 1,032,357 observations of
  - 380,753 known SSOs!

Dyn. class	#SSOs	#obs
Near-Earth	**1,652**	**2,874**
Mars-Crosser	4,242	9,024
Hungaria	6,362	12,841
Main Belt	363,188	994,812
Trojan	3,929	8,721
Centaur	123	522
KBO	1,024	3,143
Comet	233	420

Advanced photometry

A new photometry for NEAs:

- Fast-moving object from a couple of stationary SDSS sources.
- Recalculation zero-points from the reference stars.
- Photometry by elliptical apertures.
- Summarizing asteroid images for better S/N ratio.

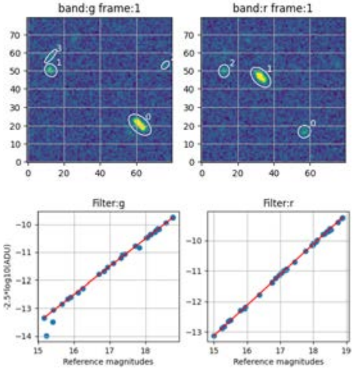

Advanced photometry

Images of the asteroid

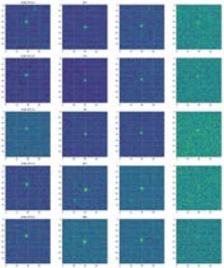

Merged image of the asteroid 2006 SP134

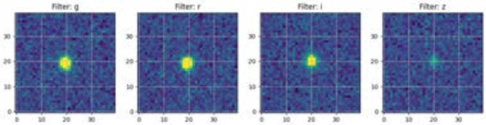

Color diagrams of the individual frames and summarised image:

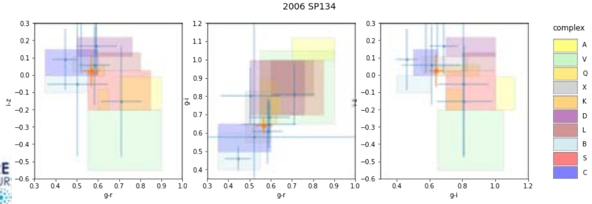

OBSERVATOIRE DE LA CÔTE D'AZUR
UNIVERSITÉ CÔTE D'AZUR

NEO ROCKS
Near Earth Object Rapid Observation, Characterization and Key Simulations

Taxonomy method

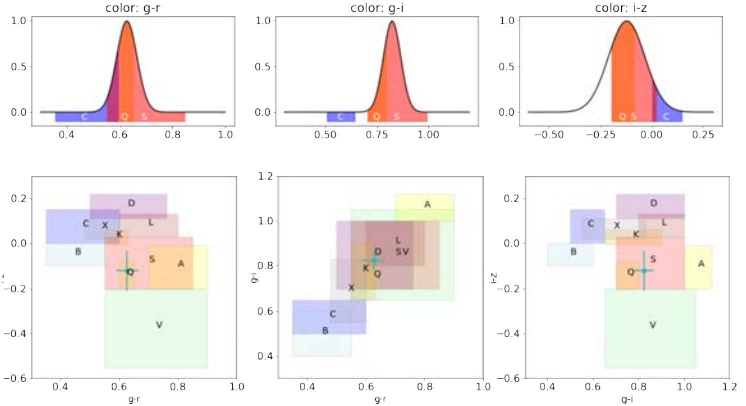

Taxonomy accuracy

Confusion matrix of the new SSOs SDSS taxonomy catalog versus published data:

Photo \ SDSS	A	B	C	D	K	L	Q	S	V	X
A	0.3	0.0	0.0	0.0	0.0	0.0	0.0	0.6	0.0	0.0
B	0.0	0.3	0.7	0.0	0.0	0.0	0.0	0.0	0.0	0.0
C	0.0	0.1	0.9	0.0	0.0	0.0	0.0	0.0	0.0	0.0
D	0.0	0.0	0.0	0.7	0.0	0.1	0.0	0.1	0.0	0.1
K	0.0	0.0	0.1	0.0	0.4	0.3	0.0	0.2	0.0	0.1
L	0.0	0.0	0.0	0.0	0.0	0.6	0.0	0.3	0.0	0.0
Q	0.0	0.0	0.0	0.0	0.0	0.0	0.6	0.4	0.0	0.0
S	0.0	0.0	0.0	0.0	0.0	0.0	0.1	0.9	0.0	0.0
V	0.0	0.0	0.0	0.0	0.0	0.0	0.1	0.1	0.8	0.0
X	0.0	0.0	0.5	0.0	0.1	0.0	0.0	0.0	0.0	0.4

Pseudo reflectance spectra of asteroids observed by SDSS, grouped by taxonomic class:

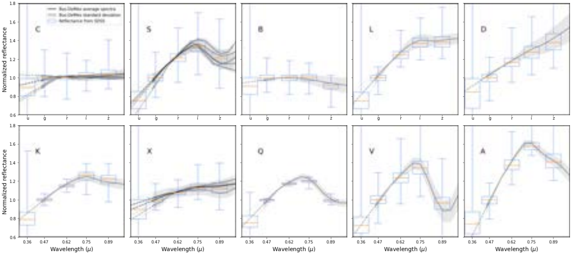

Results of NEA taxonomy

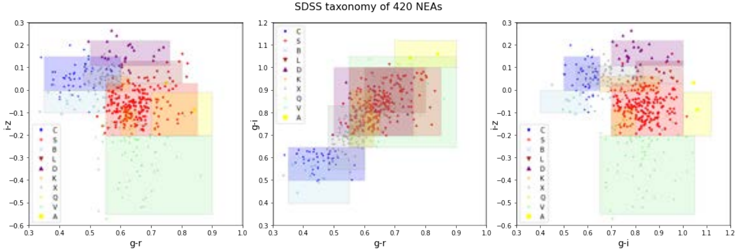

Taxonomy distribution of NEAs by dynamical classes

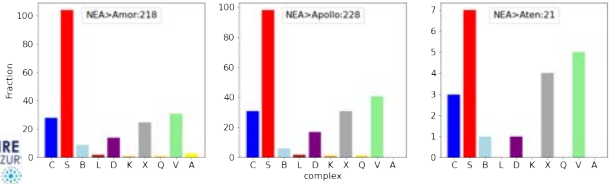

Taxonomy distribution of the probably NEA region sources*:

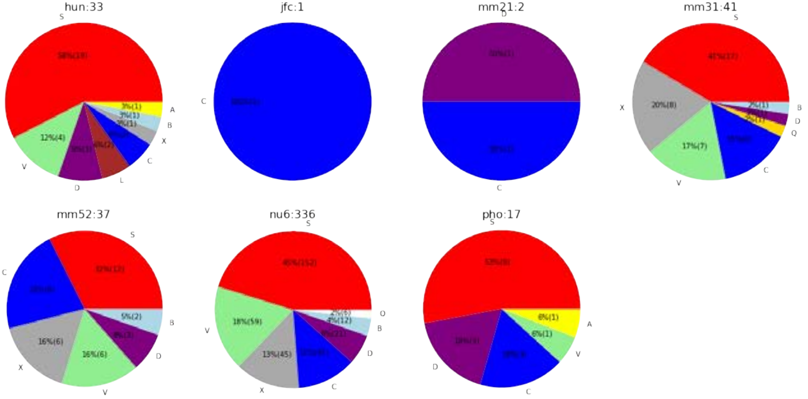

*Based on the Granvik M., Morbidelli A., Jedicke R., et al., 2018, Icar, 312, 181

Conclusion

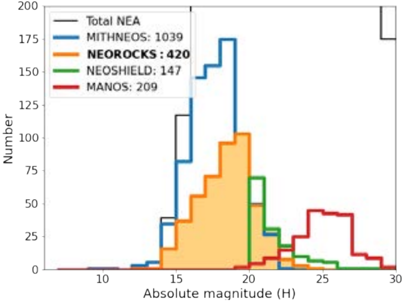

- New extraction of asteroids in the SDSS:
  - 1M observations of 300,000 asteroids
  - 1,600 NEAs + 4,200 Mars-Crossers
- Taxonomy of 420 NEAs
  - With an associated probability
  - Account for uncertainties
  - Taxonomy distribution
  - Source regions

- Future plans: Data mining in other sky surveys?
  SkyMapper, PanSTARRs, DES, LSST, Euclid, etc.

Polarimetry as a tool for physical characterization of potentially hazardous NEOs

Maxime Devogèle[1] & Nicholas Moskovitz[2]
[1]Arecibo Observatory/University of Central Florida
[2]Lowell Observatory

Planetary Defense Conference 2021
April 27, 2021

ARECIBO OBSERVATORY
PUERTO RICO
UCF · YEI · UMET

Image credit: Israel Cabrera Photography

UCF

What is polarimetry?

Measure of the linear polarization of the sun-light scattered by the surface of an asteroid

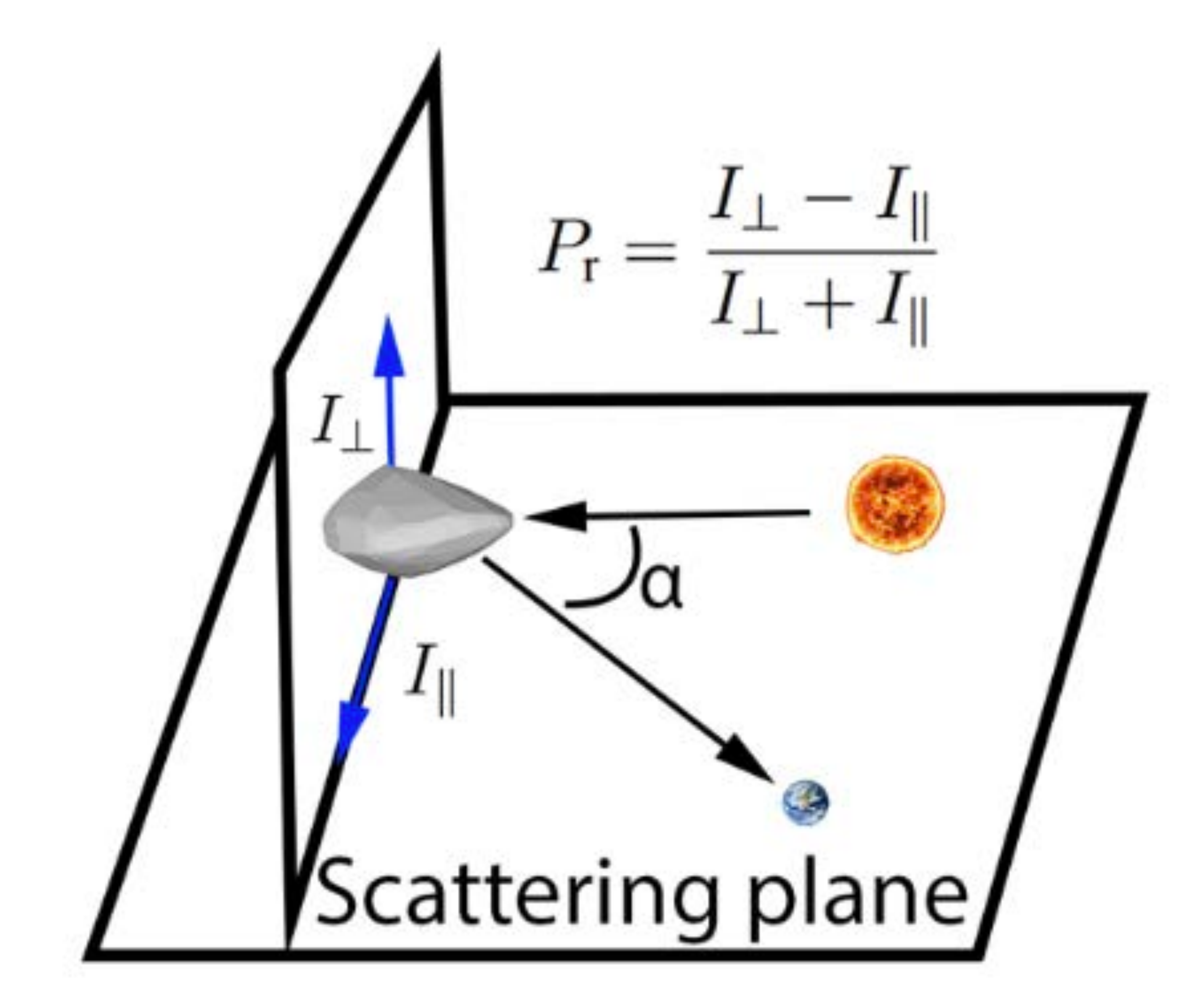

What is polarimetry?

Polarimetry is mainly dependent on the phase angle

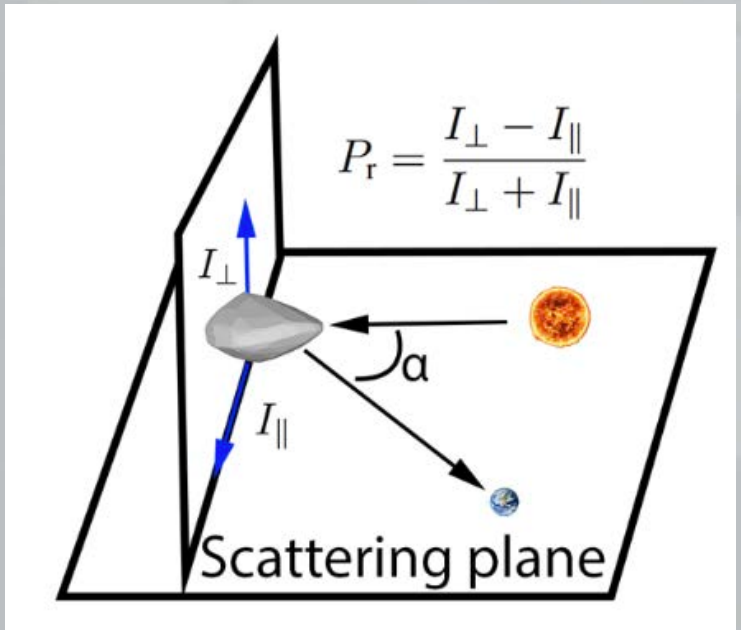

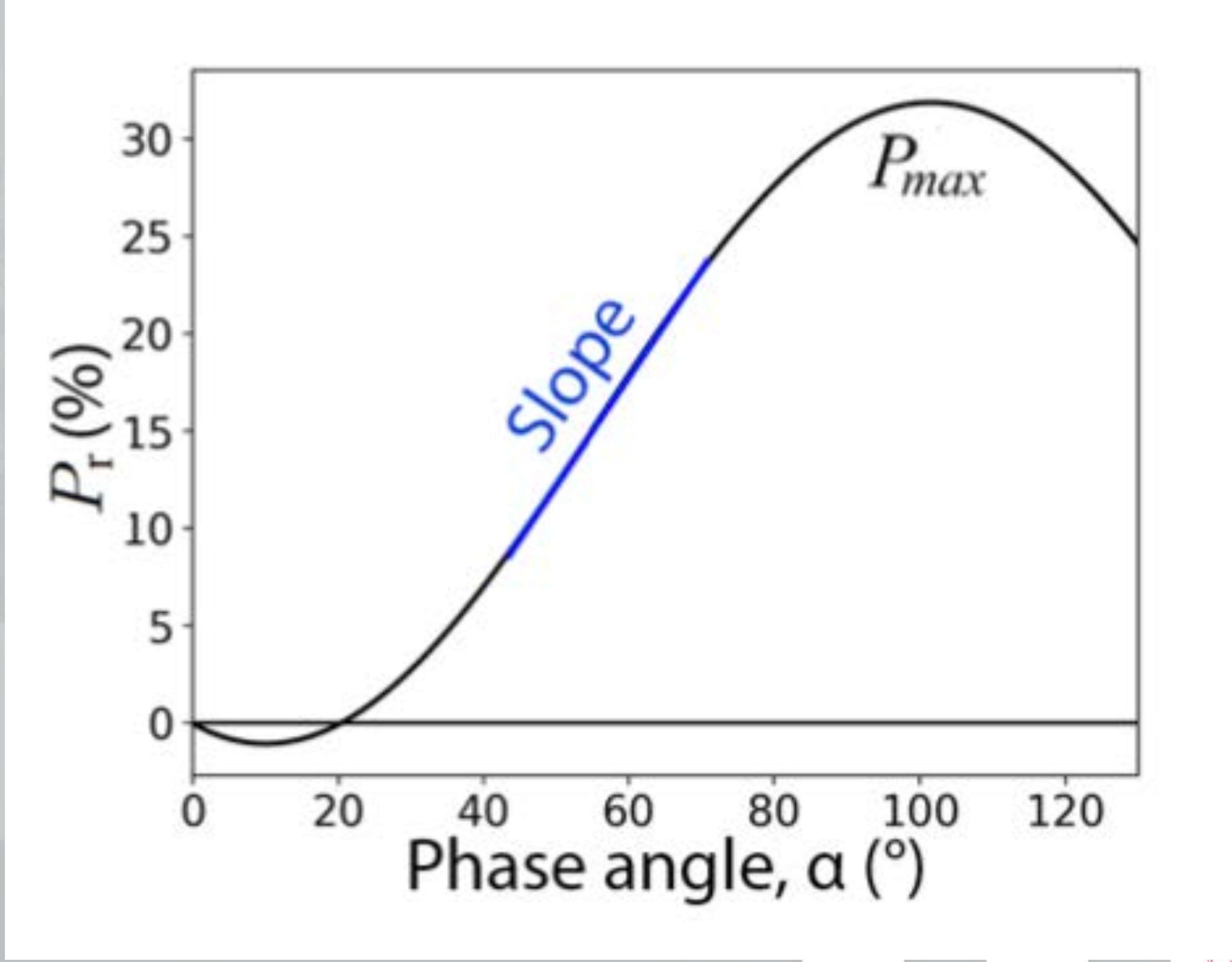

Why polarimetry is important?

The phase-polarization curve is dependent on the albedo

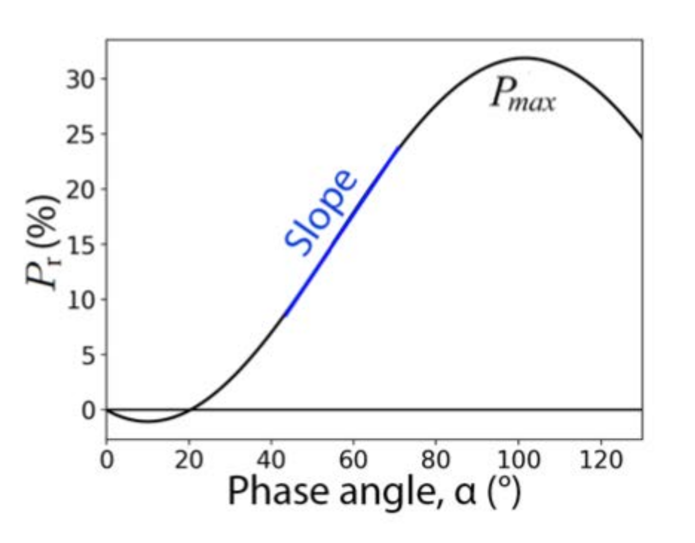

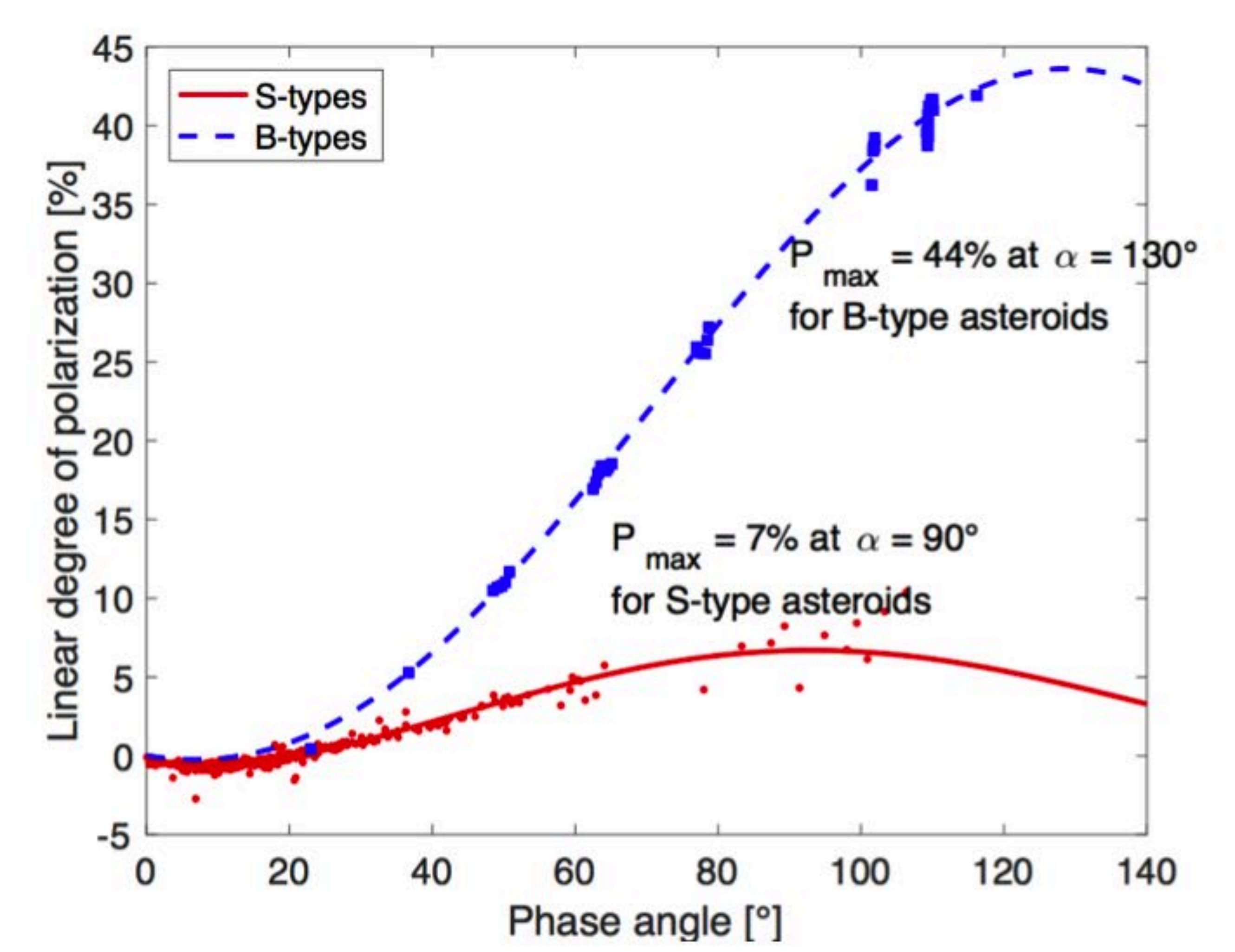

NEOs observations in polarimetry

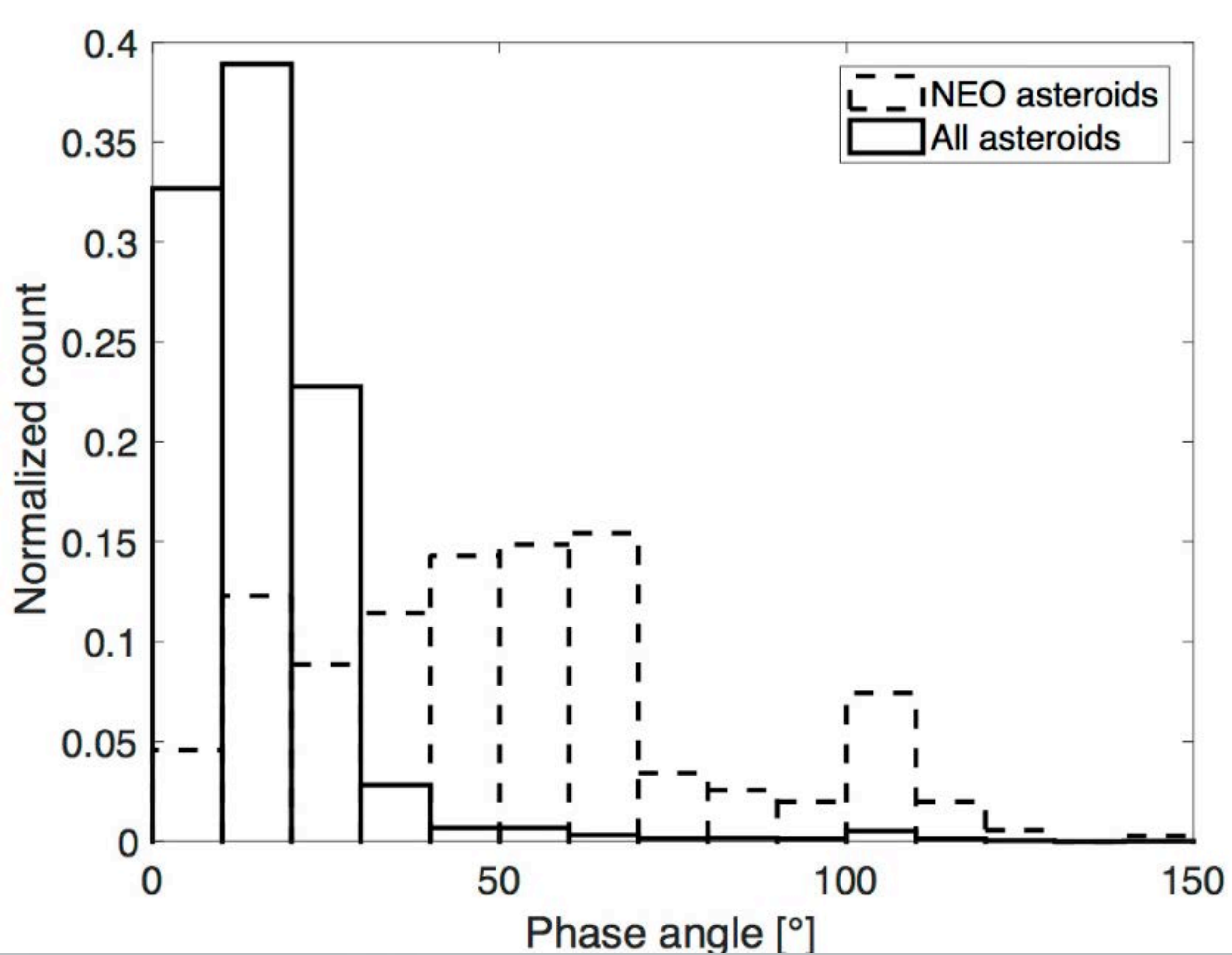

NEOs can be observed at higher phase angles

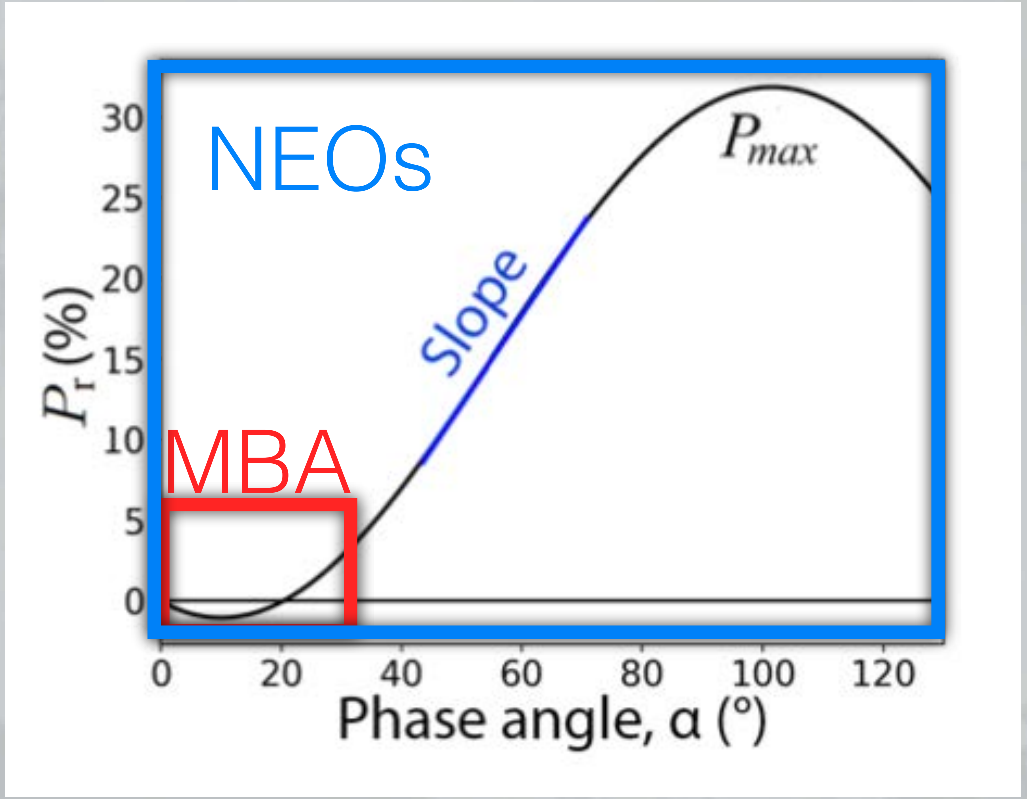

Polarimetry-Albedo relation

Bowell et al. 1973

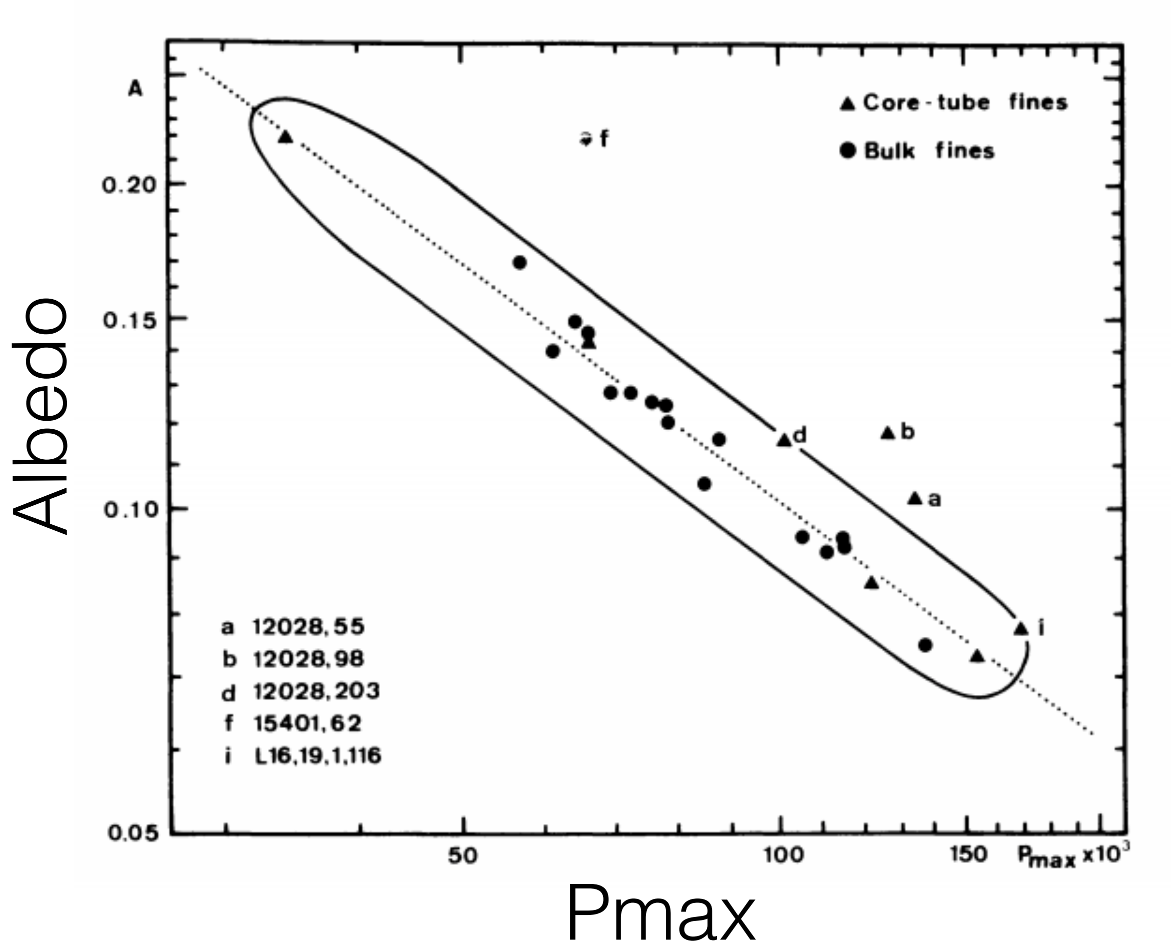

The Umov law is liking the albedo to the maximum of polarization

Polarimetry-Albedo relation

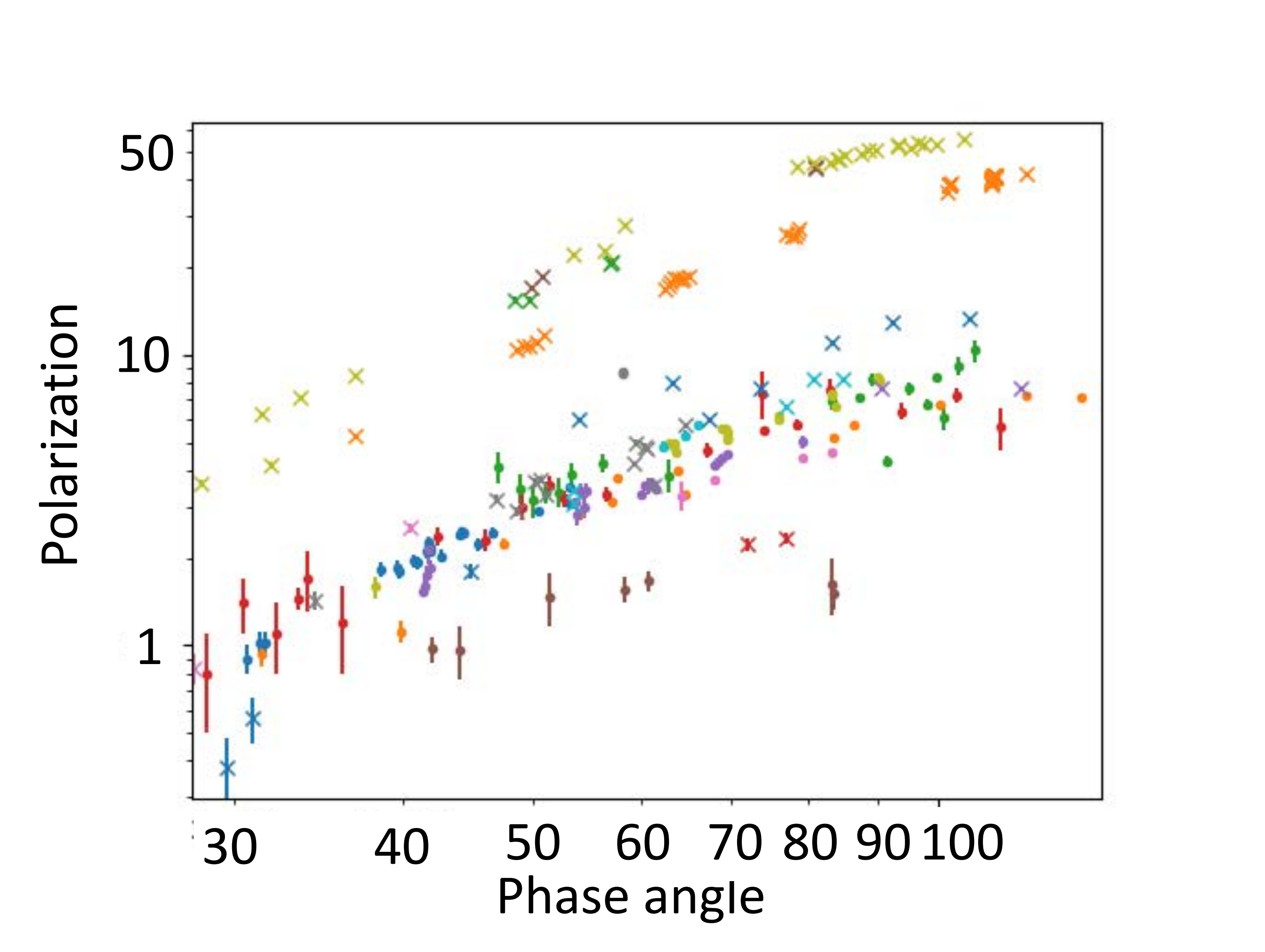

Polarimetry-Albedo relation

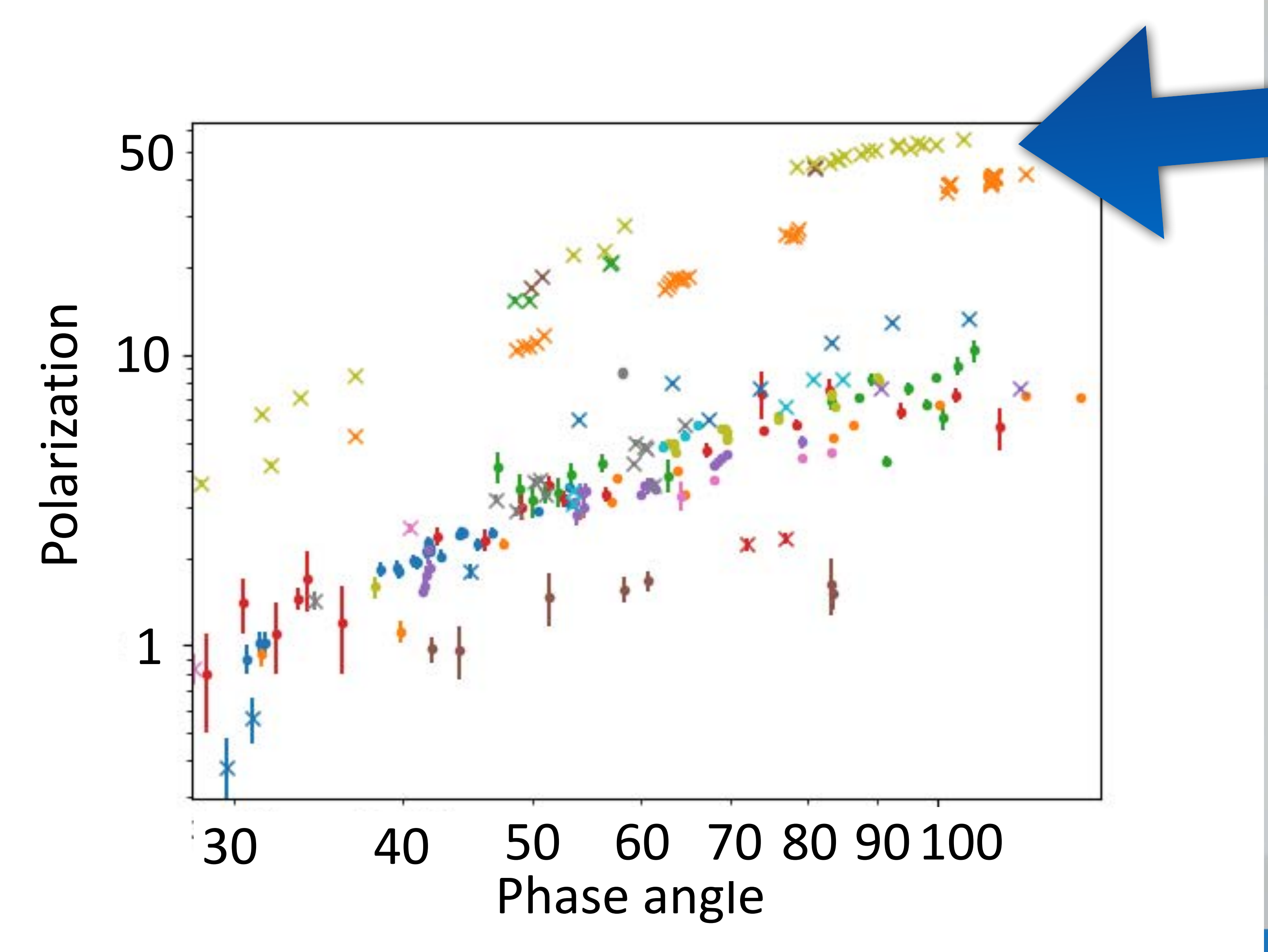

Ryugu
Bennu
1998 KU2
Phaethon

Albedo ~ 0.02 - 0.1

Polarimetry-Albedo relation

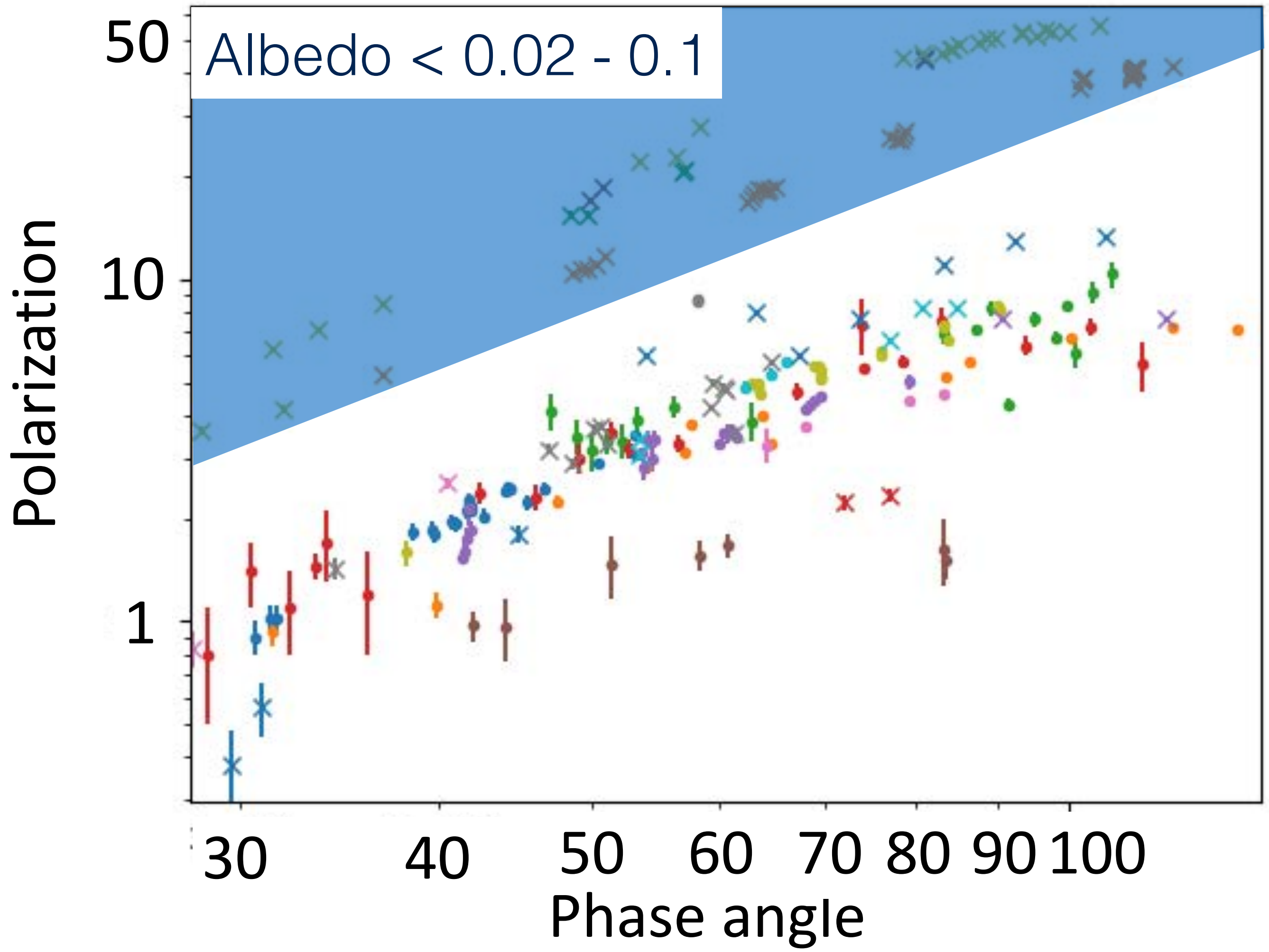

2021 PDC: 150m<D<330m

Polarimetry-Albedo relation

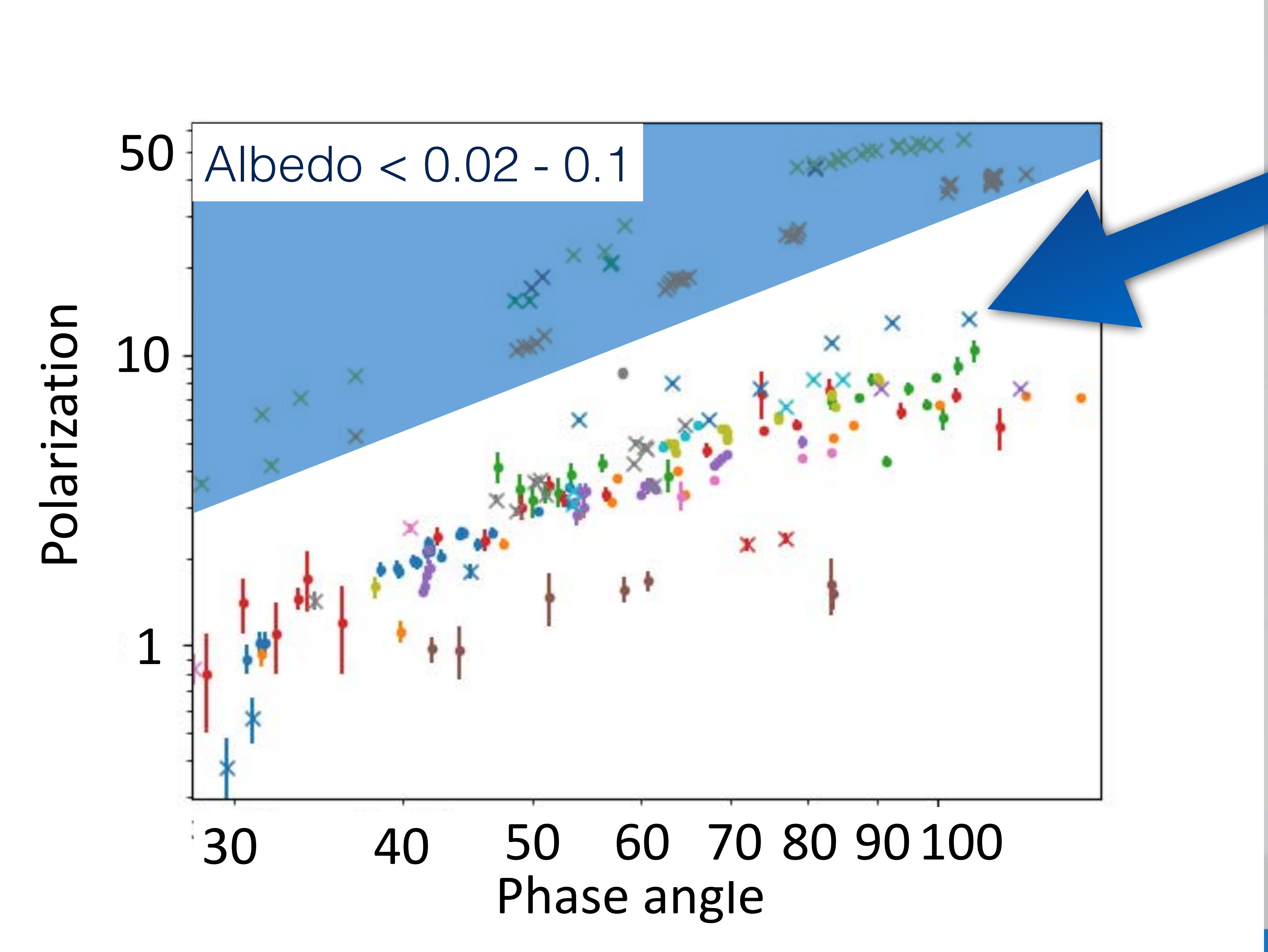

1999 JD6

Albedo ~ 0.14

Polarimetry-Albedo relation

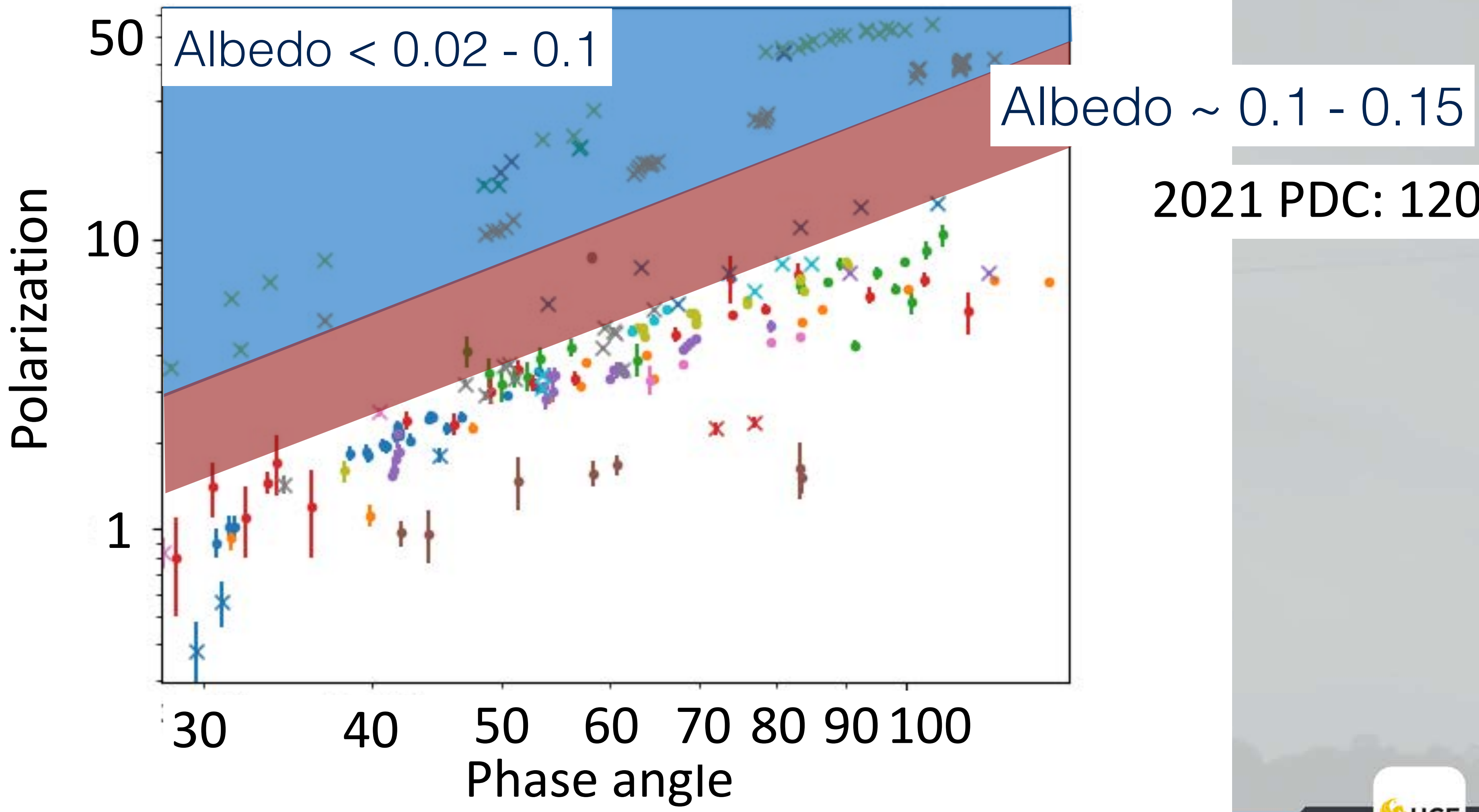

2021 PDC: 120m<D<150m

Polarimetry-Albedo relation

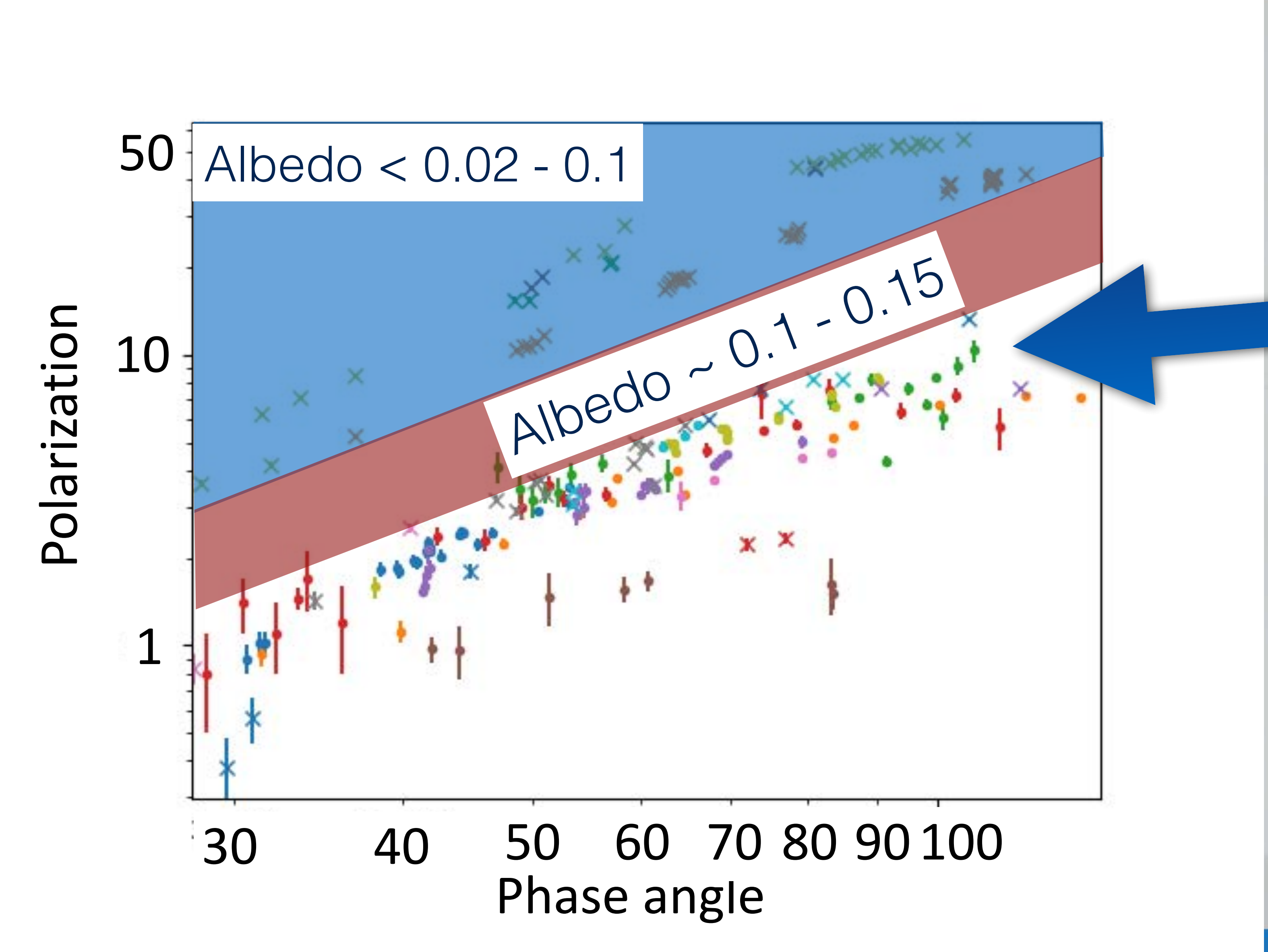

Mostly S-type
Apophis
Itokawa
Eros
Toro
Ivar
…

Albedo~
0.15-0.35

Polarimetry-Albedo relation

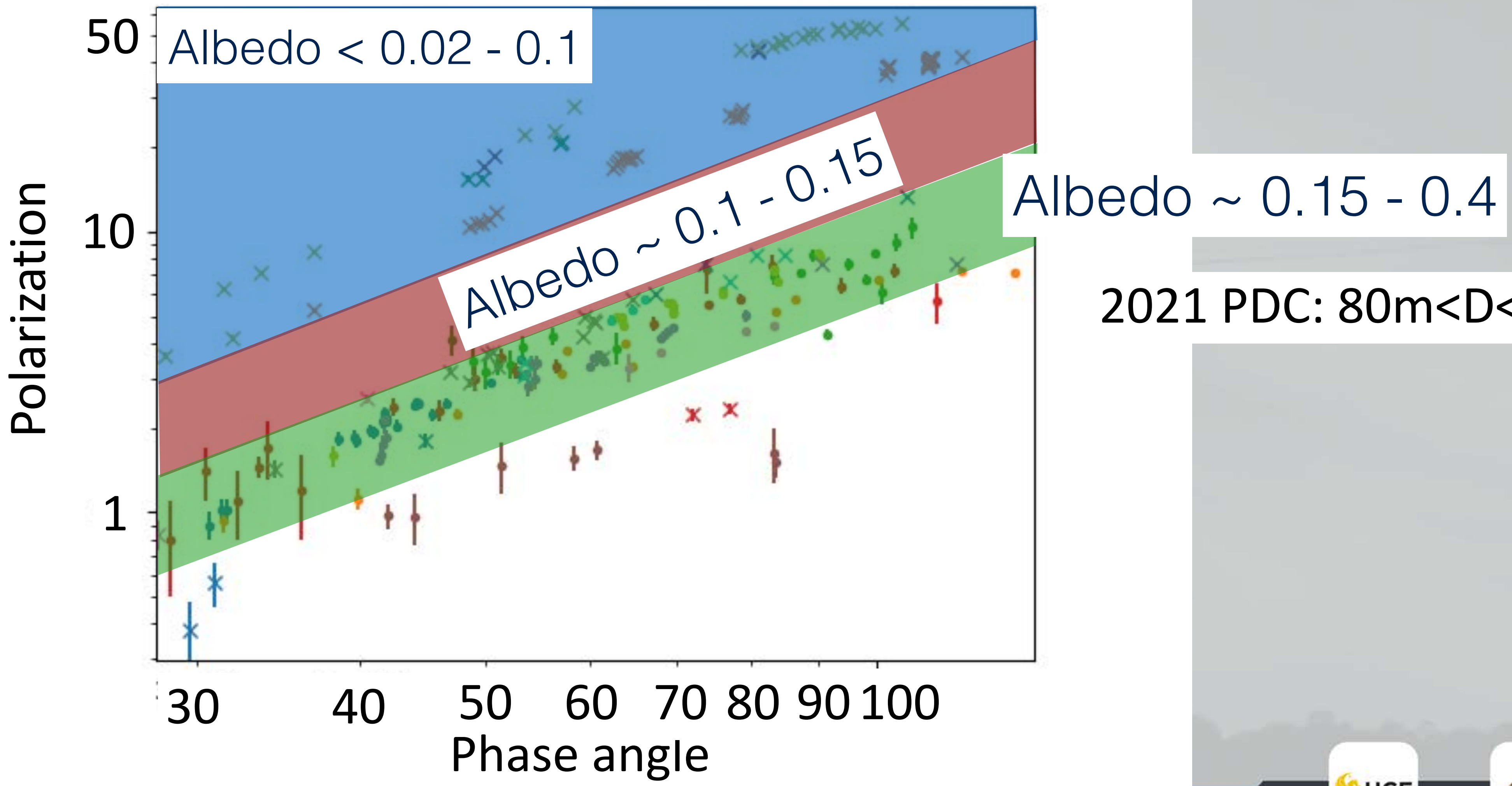

2021 PDC: 80m<D<120m

Polarimetry-Albedo relation

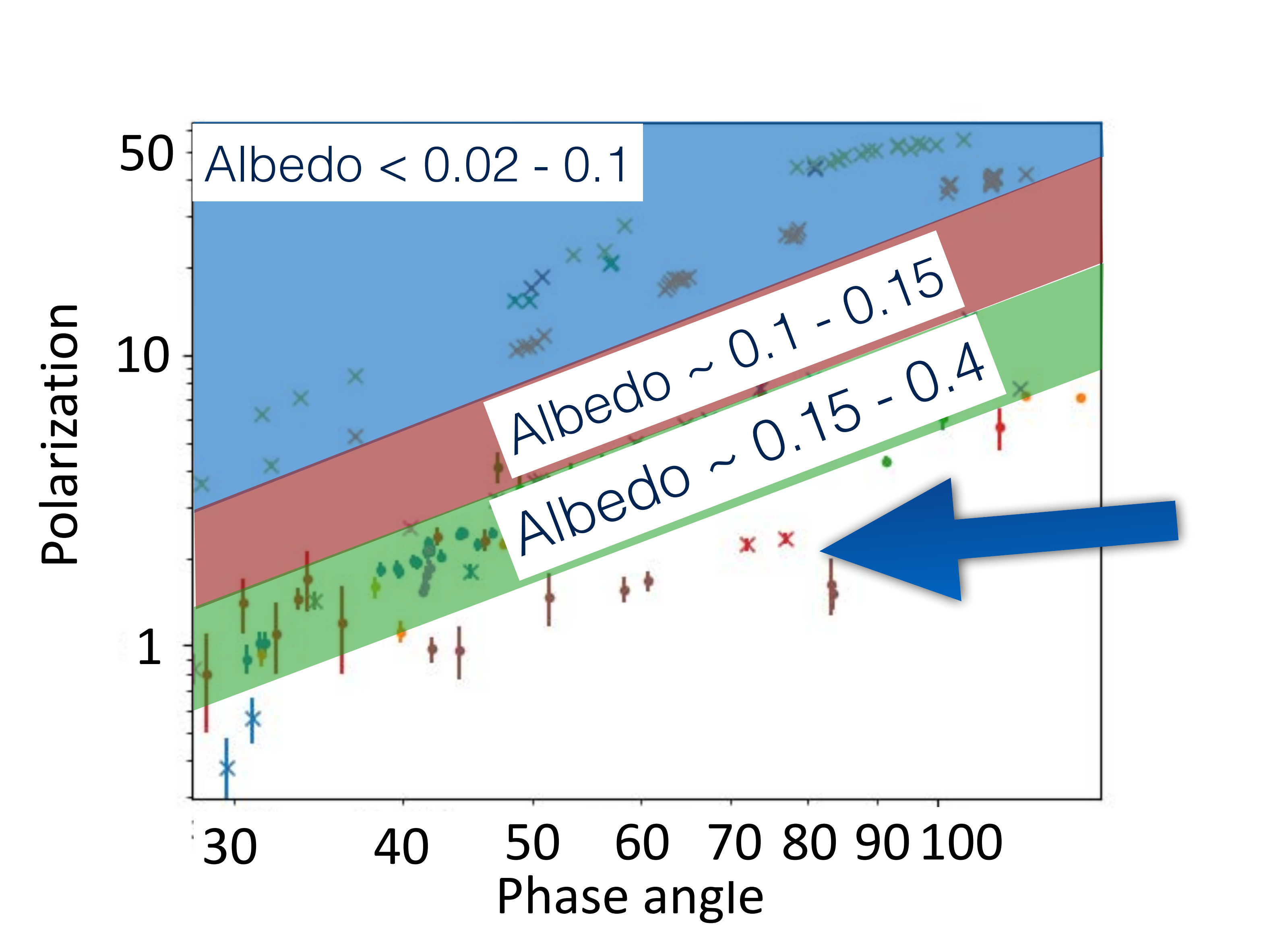

1999 WT24
2004 VD17
…

Albedo~
0.45-0.75

Polarimetry-Albedo relation

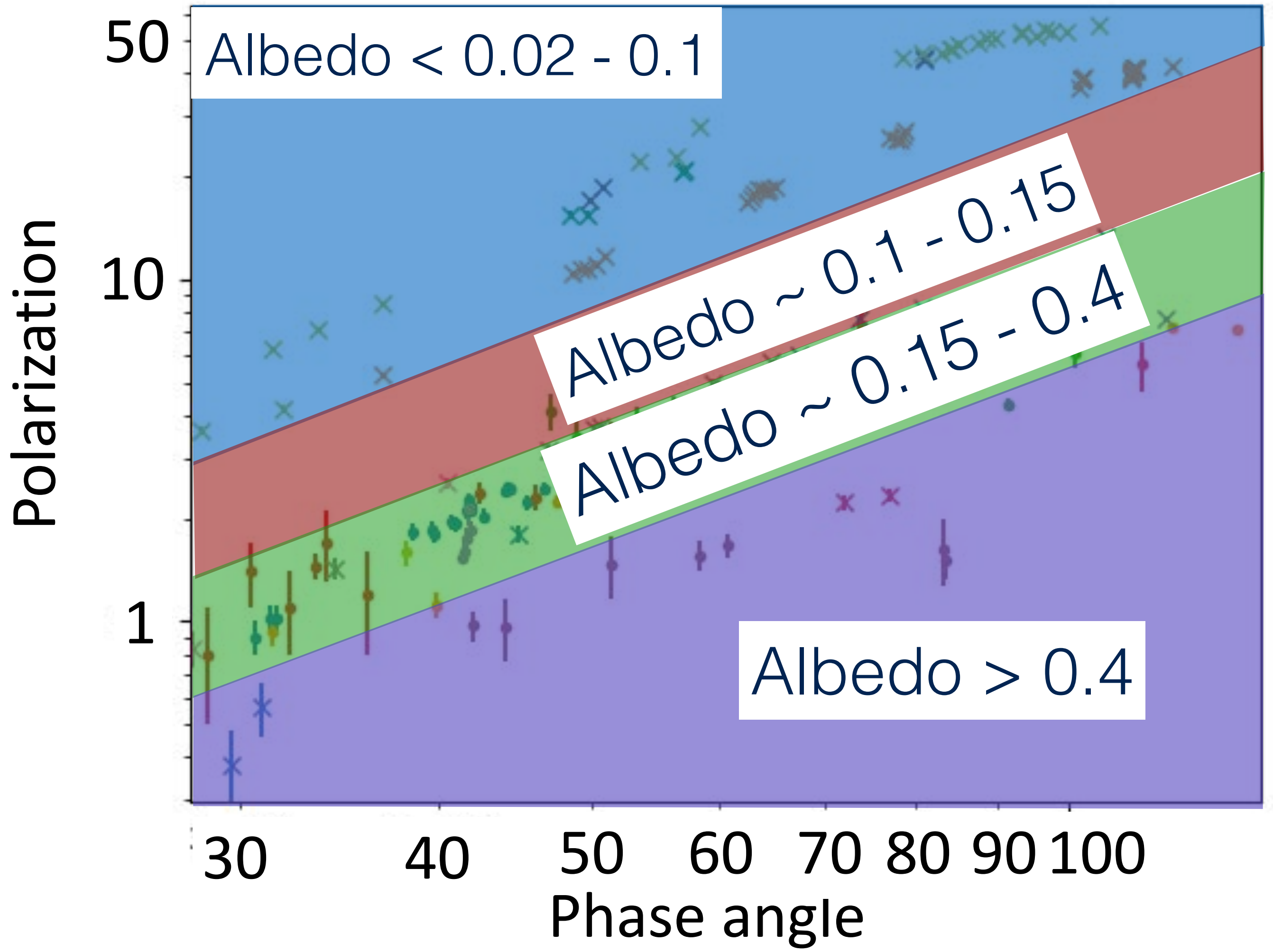

2021 PDC: 50m<D<80m

Conclusions

- Polarimetry is very effective to obtain albedo information
- One measurement can reduce the size uncertainty by a factor of 2 to 10
- We need new observations to better calibrate the polarimetry-albedo relation
- We need more polarimeters on large aperture telescopes

7th IAA Planetary Defense Conference

26-30 April 2021, Online Event

Hosted by UNOOSA in collaboration with ESA

Q&A

Session 6a: NEO Characterization

7th IAA Planetary Defense Conference

26-30 April 2021, Online Event

Hosted by UNOOSA in collaboration with ESA

Break

Up next: EXERCISE SESSION: UPDATE ON SPACE-BASED MITIGATION OPTIONS